MSc thesis

Water system analysis and numerical modelling of a coastal aquifer in western Mexico: a case study

Carlos Rosado de Palacio
July 29, 2014

Programme: Earth Surface and Water, track Hydrology
Supervisors: Dr. Ir. Gualbert Oude Essink (Deltares, Utrecht University)
                  Prof. Dr. Ruud Schotting (Utrecht University)

Table of contents

Abstract

This study combines a water system analysis of a coastal aquifer in western Mexico that is subject to seawater intrusion, where a hydrogeological characterisation of the area is given, with numerical modelling of the controlling processes and parameters as an instrument to provide a better understanding of the water system. The MOCDENS3D code is used in this study to model density dependent groundwater flow. The hydrodynamic behaviour of the coastal aquifer is similar to an island aquifer, where the freshwater lens "floats" on top of higher salinity water bodies, in this case saline from the sea and hypersaline from the lagoon. The freshwater lens varies in thickness according to the wet and dry seasons. This causes the freshwater lens to be in a delicate equilibrium between recharge and discharge of freshwater. High evaporation rates result in brine concentrations in the lagoon which enter the system in the form of saline fingers that are density driven. The numerical results provide a relatively close approximation to the density distribution that underlies the sand bar where field measurements were carried out. The results are highly sensitive to changes in the precipitation and evapotranspiration rates, with small changes leading to different concentration configurations, particularly in the freshwater lens. Results also demonstrate that a numerical model of this scale can be useful as a conceptual tool to understand the controlling factors that determine groundwater flow. The scenarios of climate change indicate that hydraulic heads will increase due to sea level rise and decrease due to longer periods of drought, and that the volume of fresh groundwater in the freshwater lens is sensitive to both of these scenarios. However, further research is necessary to provide more spatially extensive data that can be used to answer several of the uncertainties evidenced by this model.

Preface

This MSc thesis was written at Deltares in Utrecht, as a joint collaboration between Deltares and Utrecht University, under the supervision and advice of Gualbert Oude Essink of Deltares and Ruud Schotting from Utrecht University.

Acknowledgements are due to Deltares, Utrecht University and CONACYT (*Consejo Nacional de Ciencia y Tecnologia*, Mexico), without whose financial support this study would not have been possible.

I would especially like to thank Gualbert Oude Essink and Ruud Schotting, for their dedication and time and who provided knowledgeable assistance during the work and helped steer the course of this study. I would also like to thank Pieter Pauw, Sebastian Huizer and Wim de Lange for their comments and input on modelling concepts and outcomes.

Heartfelt thanks are due to my family, my mother, father and sister for their love and support. And last but not least I would like to thank Swantje Bubritzki, for her endearing love, support and encouragement for the duration of this MSc degree. Much of this work is thanks to you. You are all in my heart.

I. Introduction

I.I Background

The deteriorating effect that salinity has on freshwater reserves, in particular on coastal groundwater systems, is a pressing matter and one that has implications not only for our own benefit as human beings, but also for the environment and the sustainment of natural ecosystems (Custodio & Bruggeman, 1987; Oude Essink et al., 2010; Werner et al., 2013). Nowadays, with an extensive communication network, it is perhaps more evident than ever that we are all interdependent on each other and on the consequences of the results of previous generations, and that all our attempts to control and exploit nature and natural resources have only led our surroundings to degenerate and produce a less habitable earth. However, modern advances in science and technology seem to provide a means for restoring and preserving the natural wealth of our world.

This research project is an attempt to use the benefits of numerical modelling to better comprehend and evaluate the potential of the coastal freshwater reserves in the Western Coastal State of Sinaloa in Mexico and to provide scenarios that simulate projected climate change, including sea level rise and longer periods of drought. The study area concerns the coastal aquifer known as *Laguna Grande* in the sand bar of *Teacapan* (Figure 1).

Figure 1. Location of the coastal aquifer and *Las Cabras* study area with the model transect. Mexico map credits: Perry-Castañeda library, lib.utexas.edu (2014).

The aquifer is classified by the *Comision Nacional del Agua* (CNA, 2009) as an unconfined granular aquifer composed of sand bars that formed ancient shorelines in the presence of mixed flood plains generated by marine and fluvial processes associated with the intertidal zone. The aquifer's physical boundaries are the Pacific Ocean in the west and the *Laguna Grande* lagoon system in the north and east, therefore bound by seawater encroaching from the sea and brackish water and brine encroaching from the lagoon. This hydrodynamic system is similar to that of an island aquifer where the freshwater lens "floats" on top of saline water bodies (Figure 2).
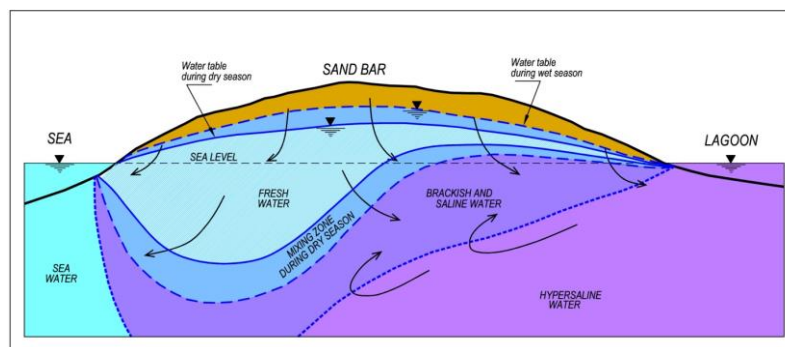

Figure 2. Schematic hydrodynamic behaviour of the aquifer in the wet and dry seasons. Rosado de Palacio (2012).

4

The data used for this study comes mainly from technical studies conducted by the consultant engineering company COPEI *Ingenieria*, based in Mexico City (COPEI *Ingenieria*, 2011). These studies were the foundation of my Bachelors thesis: "Hydrogeological Characterization of the Laguna Grande Costal Aquifer in Sinaloa, Mexico" (Rosado de Palacio, 2012). The purpose of those studies was to understand and characterize the hydrogeology of the aquifer and it's suitability for freshwater exploitation due to a large-scale tourist development project in a portion of the sand bar known as "*Las Cabras*" (Figure 1). This area has been, since 2007, a site designated by the tourism branch of the Mexican government (FONATUR) as a future large-scale tourist attraction project. It was initially named CIP (*Centro Integralmente Planeado*; Integral Planned Centre) but in 2010, following financial and environmental setbacks, the name changed to *Playa Espiritu* and the project was reduced to less built-up area and more area for nature. The project seems to be underway with slow but gradual infrastructure development.

From a hydrogeological point of view, the results in Rosado de Palacio (2012) demonstrate the presence of a thin freshwater lens, which varies seasonally and spatially with a fluctuating depth of approximately 2 to 8 m. It is recharged by rain and return irrigations of fresh water in the *Las Cabras* area. The lens is subject to evapotranspiration and agricultural exploitation mainly through surface water ditches and pumping, throughout the sand bar of *Teacapan*. This utilization (seemingly un-planned and un-ordered) and the limited availability of other freshwater sources has reduced the thickness of the freshwater lens and also induced the intrusion and mixing of saline and hypersaline water bodies from the sea and lagoon, leading to a decreased agricultural yield, to the salinization of the soil and to the subsequent deterioration of the natural ecosystem (COPEI *Ingenieria*, 2011; SEMARNAT, 2010). There is also evidence of microbiological and fertilizer contaminants in the *Las Cabras* area, originating from untreated waste-water and agricultural activities (Rosado de Palacio, 2012). It is evident therefore that there are several main issues in the area, of social, hydrological, environmental and economic nature, whereby the main stakeholders are the local fishermen and agriculturalists, the local environment and the agencies involved in the tourist development.

From a literature study, there are few other similar modelling studies that consider similar highly saline environments, where a freshwater lens is in contact with saline and hypersaline water. Studies such as that of Zimmermann et al. (2006) show the result of modelling brine formation on islands. The study of Kafri et al. (2013) shows similar results to this study.

I.II. Scope of this study

The scope of this study is to better understand the hydrogeological processes affecting the vulnerability of freshwater reserves in the freshwater lens by means of a numerical model that simulates the complex dynamic system of a coastal aquifer, including the fresh-salt-brine water relations and the factors that apparently drive these changes. The model can then be used as a platform for simulating scenarios of changes to the system, i.e. Climate change and sea level rise. These scenarios will be presented in the results section below.

II. Available data

The available data, as mentioned previously, comes from technical studies of COPEI *Ingenieria*, 2011, which were integrated in the study of Rosado de Palacio, (2012). In these studies, the hydrogeology of the *Las Cabras* site was used as representative for the entire aquifer system given the similar hydrogeological and stratigraphic dispositions of subsurface units, although measurements were carried out throughout the *Teacapan* sand bar and beyond in the lagoon wetland system and neighbouring towns.

Hydrostratigraphy

The study in Rosado de Palacio (2012) provided a general overview of the regional geology and hydrostratigraphy of the area which was verified by field visits and geophysical surveys. The size and shape of the freshwater lens and the distribution of saline water bodies in the subsurface was characterised with piezometric measurements and salinity profiles and indirectly with the aid of geophysical surveys. Figure 3 shows a schematic representation of the hydrostratigraphy of the area and the different units, structured according to the storage and transmission of groundwater. The Laguna Grande coastal aquifer is found in Unit 1 between the sea and the lagoon, it is composed of gravel, sand, silt originating from accretion bars.
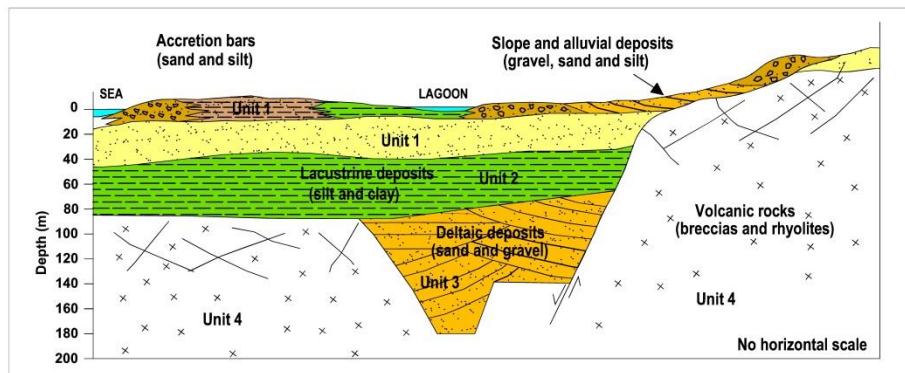

Figure 3. Schematic representation of the hydrostratigraphic units and their possible arrangement in the subsurface. Rosado de Palacio (2012).

Geophysical surveys

Six TEM (Transient ElectroMagnetic) lines were established in April 2009, under the supervision of COPEI *Ingenieria*. The purpose of the TEM-survey was to measure the geoelectric response, for lithology and water salinity, of the subsurface units in an area encompassing the *Las Cabras* site, the lagoon wetland system and the three nearest towns to the study area (Figure 4). A geoelectric profile was generated for each line, which includes two or more TEM's, in which by means of colours and resistivity values it was possible to group different units in the subsurface, based on their geoelectric response. The possible lithological and hydrogeological correlation of the units is integrated in a table which is shown below each profile.
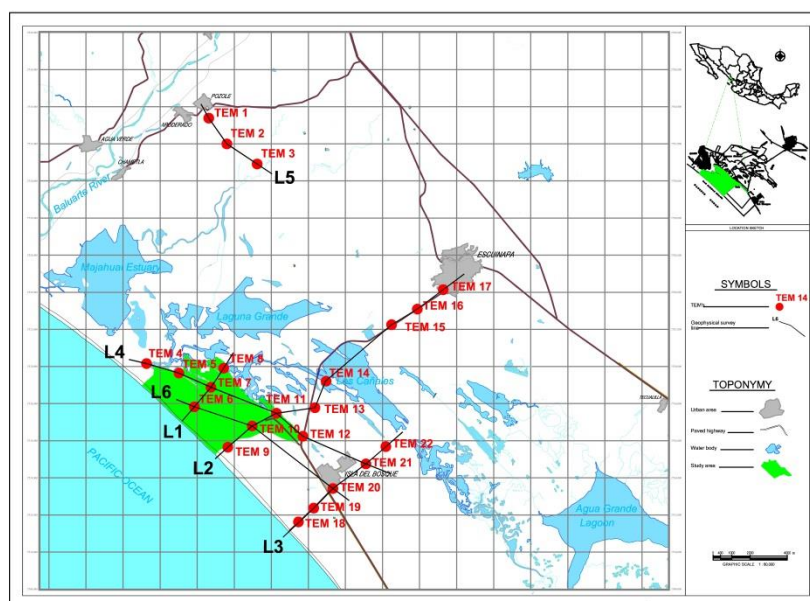

Figure 4. Location of the interpreted geophysical profiles. Rosado de Palacio, 2012.

6

For the purpose of this study, only lines one (L1) and two (L2) are shown since L1 is the most complete in terms of interpretation and L2 is the longest profile. In L1, more information about the subsurface is available in that area and therefore can be correlated directly with exploratory boreholes and salinity profiles, which were measured in three wells (B1, B2 and B3) located in the same spot where TEM's 6, 7 and 8 were laid out, respectively. This profile, shown in Figure 5, integrates data from depth to the water table, salinity profiles measured in three periods (two during the dry seasons and one during the wet season), the mixing zone between fresh, brackish, saline and hypersaline water (see Table 1), the lithological cross section of the three exploratory boreholes (B1, B2 and B3) and the correlation of a high permeability interval between the three wells. This profile shows the possible stratification of subsurface geological units and water bodies of different salinity. U1a, which can also be correlated with Unit 1 in Figure 3, is the unit where the freshwater lens is located, with resistivity values that are in accordance with direct salinity measurements in well B1 (TEM6). It is underlain by U2 which shows resistivity values that indicate saline and hypersaline water bodies, where the salinity starts to increase sharply from a depth of 5 m as evidenced in well B2 (TEM7). Note the dilution of salt in the salinity profiles between the dry and wet periods (this issue is addressed in more detail in the section of Salinity Profiles below). In well B3 (TEM8), the influence of high salinity from the lagoon is visible in the resistivity and EC values. These show a sharp increase in salinity from a depth of 5 to 6 m until the EC exceeds 100,000 µS/cm (detection limit of the Hydrolab probe) at 10 or 15 m. No significant change is observed in well B3 between the three measurement periods, suggesting that the hypersalinity remains relatively constant throughout the year. Unit U3 denotes the possible bedrock, composed of fractured volcanic rocks, which were recovered in core samples at a depth of –88 m.b.s.l and are described in Rosado de Palacio (2012).

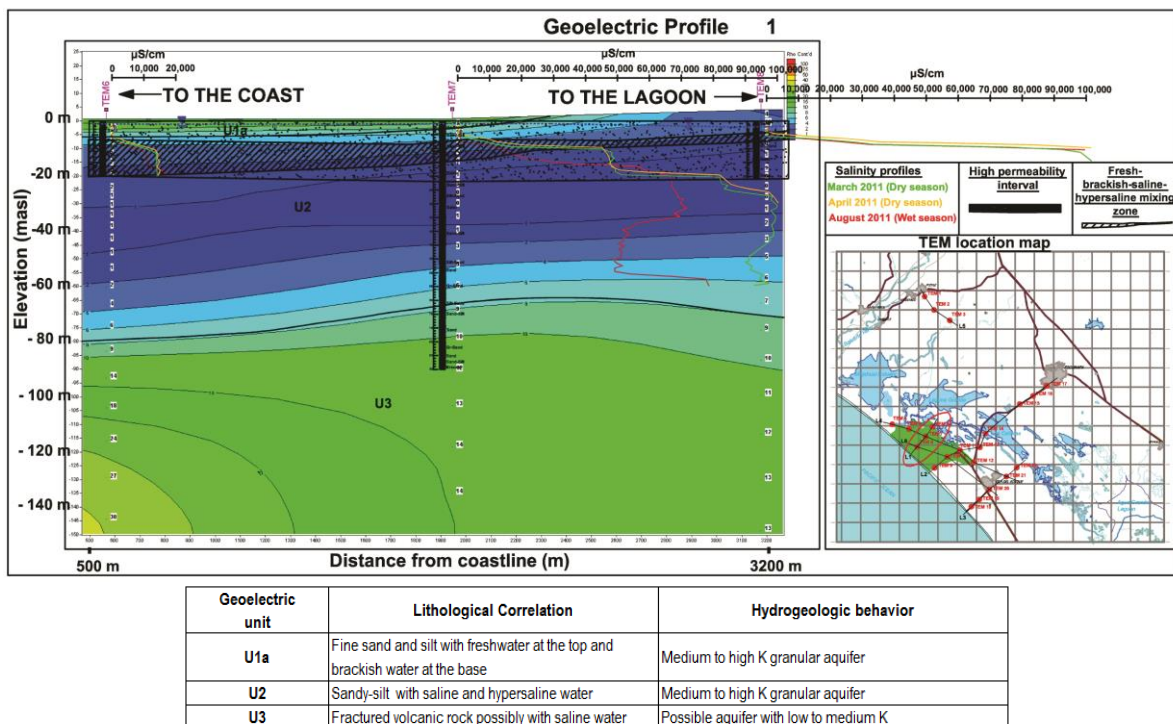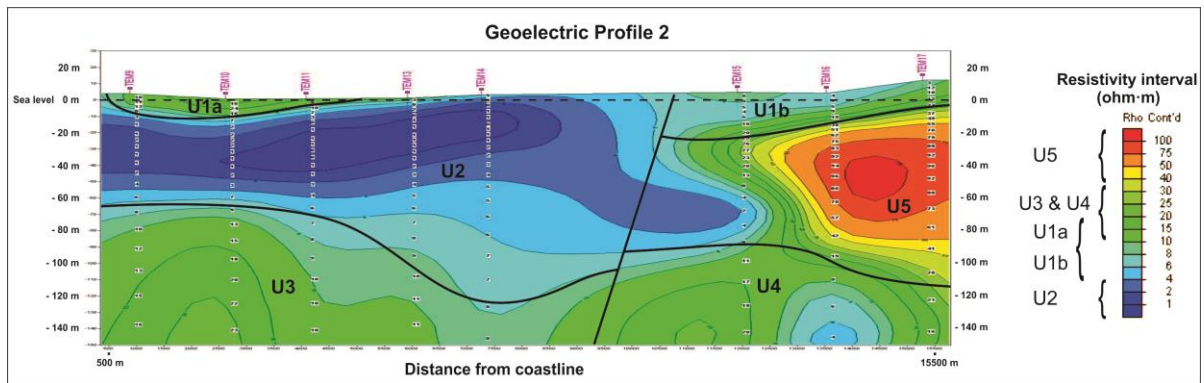| Geoelectric unit	Lithological Correlation	Hydrogeologic behavior
U1a	Fine sand and silt with freshwater at the top and brackish water at the base	Medium to high K granular aquifer
U2	Sandy-silt with saline and hypersaline water	Medium to high K granular aquifer
U3	Fractured volcanic rock possibly with saline water	Possible aquifer with low to medium K

Figure 5. Geoelectric profile 1 (L1). Rosado de Palacio, 2012.

L2, in Figure 6 below, is the longest profile and includes the area of the freshwater lens, the higher salinity lagoon and a portion of land adjacent to the lagoon system. Five geoelectric units can be identified in L2. The freshwater lens, underlain by brackish water can be correlated in unit U1a and U2 shows the possible shape and extent of the saline and hypersaline water bodies. From this profile, a hydrogeological correlation can be established between U1a, U1b and U2 with Units 1, 2 and 3 and between U4 and U5 with Unit 4 of the hydrostratigraphic representation in Figure 3.

Geoelectric unit	Lithological Correlation	Hydrogeologic behavior
U1a	Fine sand and silt with freshwater at the top and brackish water at the base	Medium to high K granular aquifer
U1b	Fine sand with brackish water	Medium to high K granular aquifer
U2	Sandy-silt with saline and hypersaline water	Medium to high K granular aquifer
U3	Fractured volcanic rock possibly with saline water	Possible aquifer with low to medium K
U4	More compact volcanic rock possibly with saline water	Possible aquifer with low K
U5	Low permeability rock	Low K aquitard

Figure 6. Geoelectric profile 2 (L2) and table with lithological and hydrological correlation.

Pumping test

A pumping test was carried out in the study area in April 2010, for a total continuous pumping time of 24 hours. The interpretation of the pumping test provided the parameters of hydraulic conductivity (K), transmissivity (T) and specific yield (Sy). The interpretation included the drawdown which occurred in the observation well, located 8 m from the pumping well, and the recovery, with the latter shedding more precise data. The saturated thickness (b) was taken as the approximate thickness of the freshwater lens (10 m), because for the purpose of the study of Rosado de Palacio (2012), this would be the exploited interval of the aquifer.

The data obtained from the recovery phase is: approximately 40 m/day for the hydraulic conductivity, 400 m^2/day for transmissivity and 0.12 for specific yield (Rosado de Palacio, 2012). The hydraulic conductivity values are correlated with medium to coarse sands and are therefore given a qualitative rating of high conductivity. Being an unconfined aquifer, Sy = effective porosity (ϕ_{EF}), therefore ϕ_{EF}=12% which is equivalent to sand and loose gravel.

Head measurements

Groundwater head measurements were carried out in a piezometric survey during October of 2002 by CNA, which corresponds to the end of the wet season (CNA, 2009). The results of this study identified a hydraulic gradient where the groundwater flows from the higher terrain elevations towards the lagoon; and in the area of the sand bar, the flow occurs from the central portion and discharges towards the lagoon and sea boundary (Figure 7**a**). Additionally, the study found that in the sand bar, groundwater heads are low and close to sea level, which implies that there is virtually no groundwater discharge into the sea. In more recent years, and derived from the study of Rosado de Palacio (2012), a monitoring network was established for the *Laguna Grande* aquifer, where groundwater head configurations were elaborated for different measurement periods. In Figure 7**c**, a schematic representation of the groundwater flow is presented along with the groundwater head configurations for October 2002 and August 2011, the latter being representative of the general shape of the potentiometric lines in the area of *Las Cabras*. Note the dome shaped watershed in the sand bar in figures 7**a** and 7**b**, where groundwater flows radially towards the sea and lagoon boundaries. The figures also show where groundwater extraction is more pronounced, creating a cone of depression, which, in the southern portion of the sand bar, is even below sea level.

Two weather stations were used for the interpretation of rainfall and evapotranspiration data in the study area. The *Acaponeta* weather station is 115 km from the study area and the *La Concha* weather

station is 50 km from the study area. Both stations record daily precipitation and temperature and the *La Concha* station records also evapotranspiration rates.
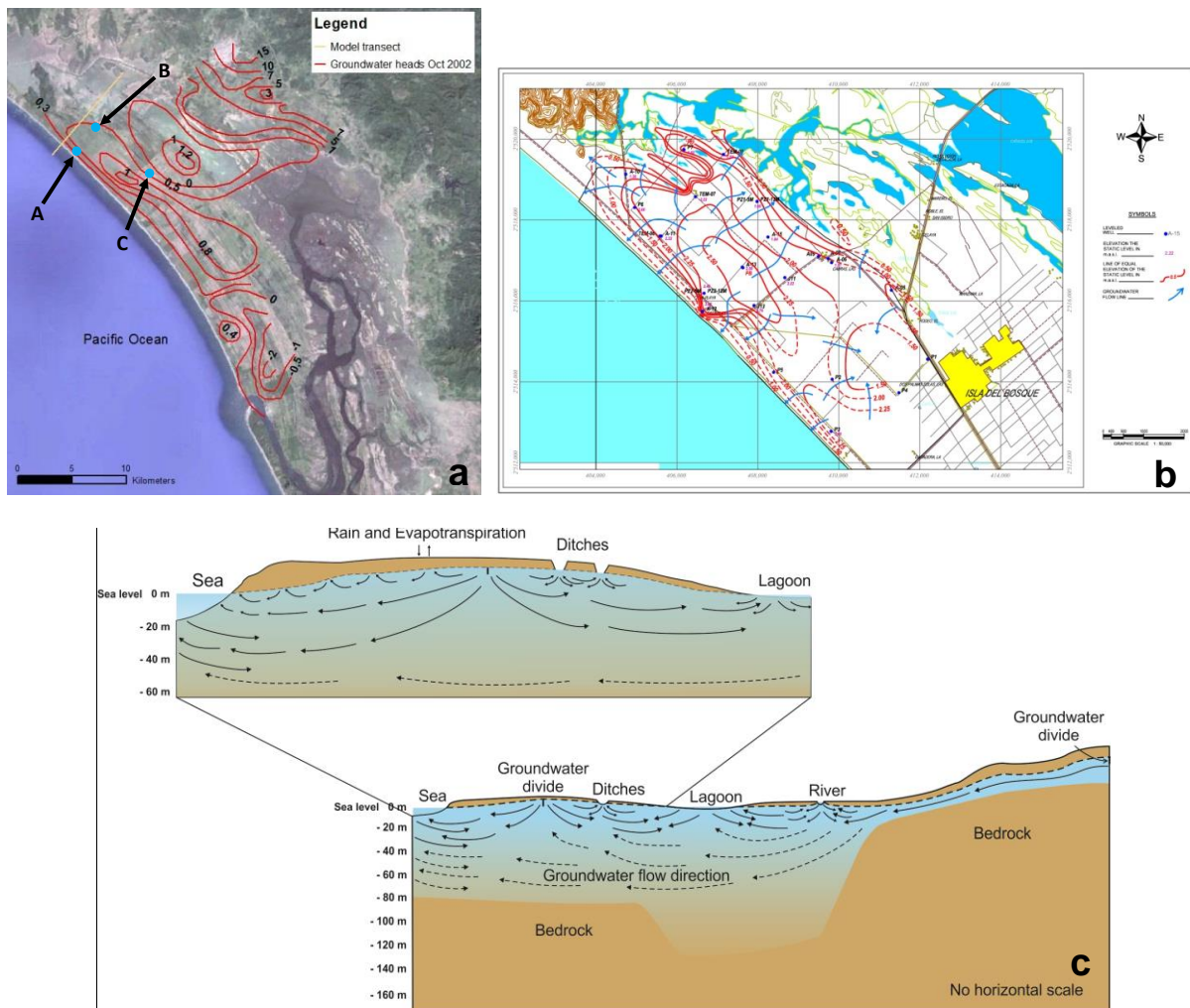

Figure 7. Equipotential lines representing groundwater head measured in **a** October 2002 and **b** August 2011, equivalent to the beginning of the dry season and the middle of the wet season respectively. Location of piezometers A, B and C in **a**. Dashed lines represent the inferred position of potentiometric lines in **b**, and the inferred flow direction in **c**. **c** is a schematic representation of groundwater flow direction in the study area. Source of **b** is Rosado de Palacio, 2012.

Punctual seasonal groundwater variations were recorded with pressure transducers or divers in piezometers A, B and C (Figure 7**a**) from March to August 2011. The resulting graphs below (Figure 8) display the seasonally influenced groundwater head, where variations between seasons in this portion of the sandbar fluctuate between 0.60 m and 0.70 m. Note also the quick recovery of the water table in accordance with the wet season. The daily rainfall graph from the *Acaponeta* weather station (115 km from the study area), shows the dry season (March-June) followed by the wet season (July-August).

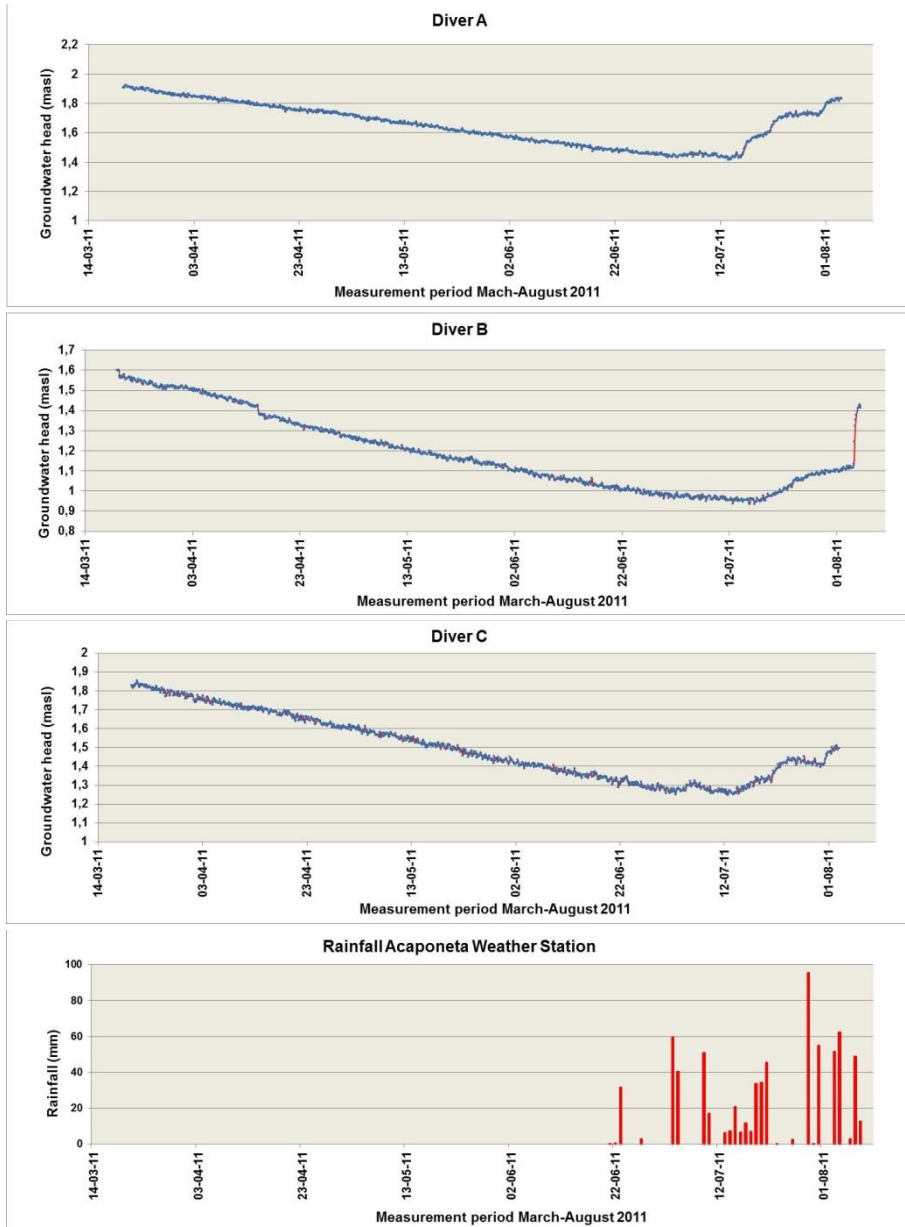Figure 8. Seasonal groundwater head fluctuations in three piezometers in the sand bar and rainfall measurements in the Acaponeta weather station.

In Figure 9, the graphs of average annual precipitation and evapotranspiration in the *La Concha* weather station from 1962 to 2008 are shown. Evapotranspiration is larger than precipitation throughout the year, in many cases exceeding by double the amount of precipitation.
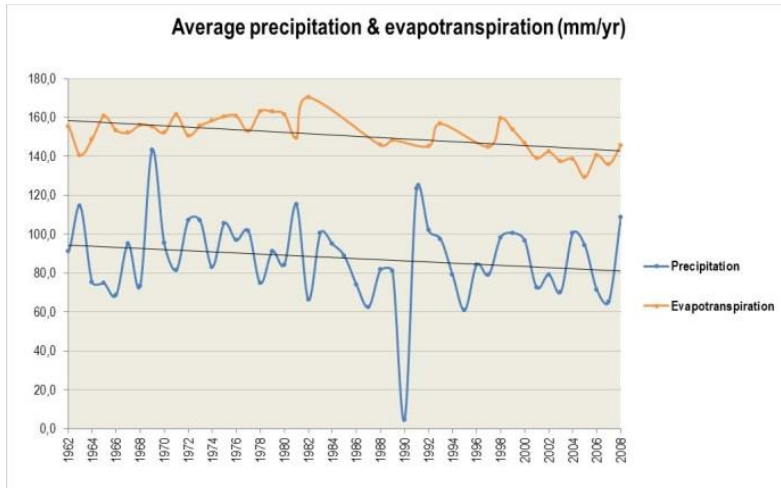
Figure 9. Average annual precipitation and evapotranspiration in the *La Concha* weather station.

Salinity profiles

Three measurement periods of salinity profiles were available in 2011, two in the dry season (March and April) and one in the wet season (August). Profiles were measured from the water table to the drilled depth of the well (except in well B2 where the probe could not pass after 60 m.b.s.l, possibly because of a bent well casing), using a Hydrolab Quanta-G probe with a detection limit of 100,000 µS/cm of electrical conductivity. These measurements are displayed in Figure 5 above, where they are integrated with other data; below however, they are displayed individually for greater detail and comparison purposes. In each measurement period, a small map indicates the location of the well along with an indicator of seawater conductivity.
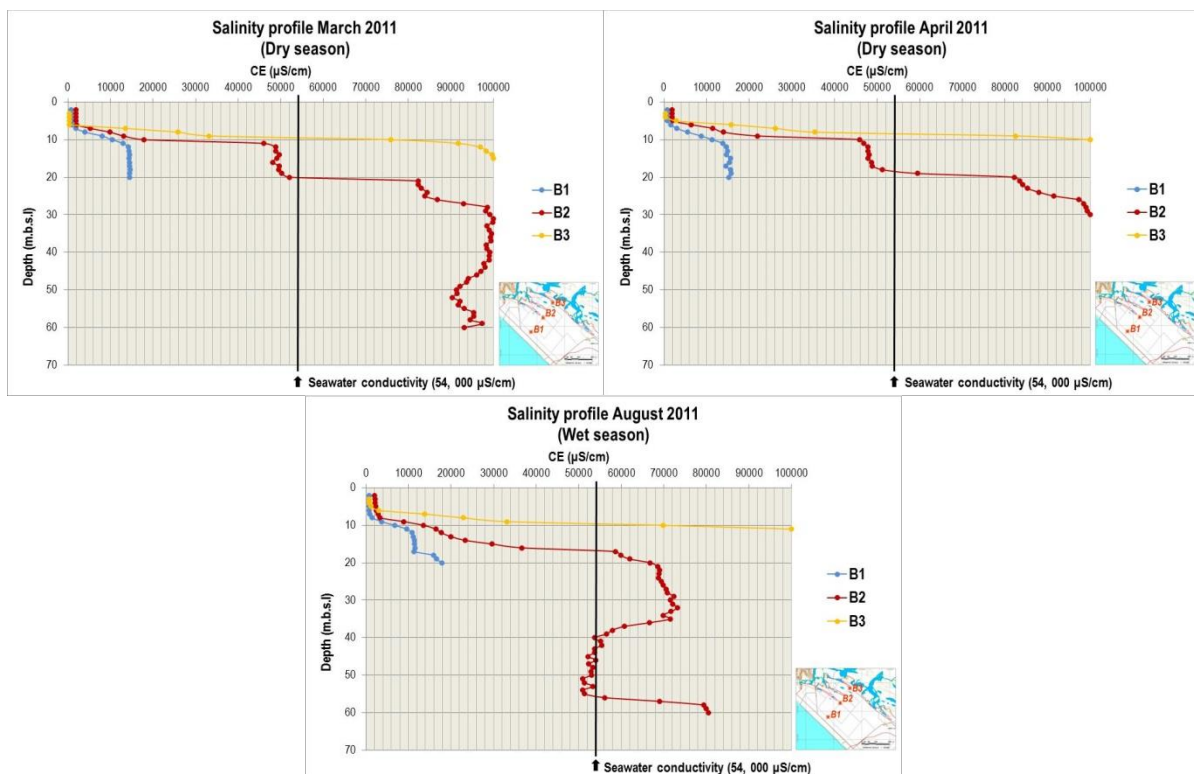

Figure 10. Salinity profiles on three measurement periods in observation wells B1, B2 and B3 during 2011. Rosado de Palacio, 2012.

From these profiles, it is evident that well B1, closer to the coastline, has the greatest depth of the freshwater lens, with a relatively constant thickness of 6 to 8 m between seasons. In the middle section of the sand bar, where B2 is located, there is a thinner freshwater lens which is more responsive to increases in salinity. Details of these EC seasonal variations can be found in Annex 2. The vertical depth of the lens varies here between seasons, from virtually zero in the dry season to 4 or 5 m during the wet season (Detail in Annex 2). The influence of hypersaline water is evident in this profile, with values of EC higher than seawater (> 54,000 µS/cm) occurring from a depth of 20 m.b.s.l onwards. The rapid response in dilution of salinity which is observed in this profile, especially from a depth of 20 to 60 m.b.s.l, suggests that the geological environment could be highly permeable and consistent with the results of the pumping test. It is also indicative of a possible influence of freshwater coming from the inland hills and mountains, as indicated in Figure 7**c**. In well B3, closer to the lagoon system, there is a clear influence of hypersaline water from the lagoon causing a sudden increase in salinity from a depth of 5 to 6 m.b.s.l, where the detection limit of the Hydrolab probe is exceeded. The freshwater lens in this area fluctuates between 2 and 4 m. The mixing zone between fresh-brackish-saline-hypersaline is thickest closer to the coastline and in the mid-section of the sand bar, and in the lagoon boundary there is a sharp interface where freshwater is almost immediately underlain by hypersaline water. These findings can be schematised as Figure 11 below.
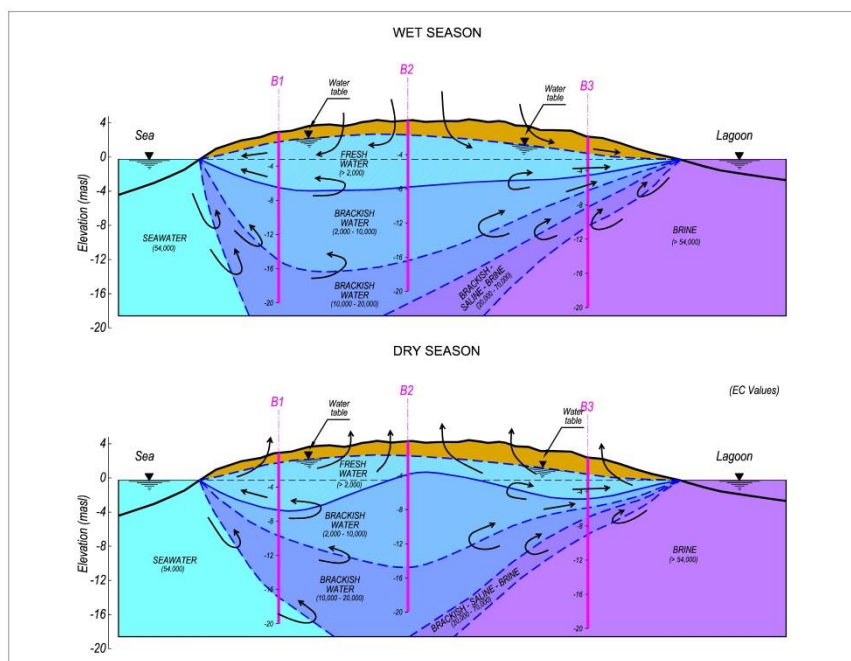
Figure 11. Schematic representation of the salinity variation in the first 20 m.b.s.l between the wet and dry seasons based on salinity profiles.

It is important to point out that the aquifer is highly responsive to periods of rain and evapotranspiration, which themselves are highly transient and vary from year to year.

Water quality

In April 2011, a sampling of surface and groundwater was conducted in the *Las Cabras* area. As mentioned in Rosado de Palacio (2012), almost all sampled sites have coliforms (total and faecal), indicative of contamination by human waste. Additionally, several sampled sites present high values of Sodium, Iron, Fluoride, Manganese and Total Dissolved Solids. These findings were plotted in Stiff diagrams, which characterize the geochemistry of the groundwater. Figure 12 below shows the results of the Stiff diagrams and the different water families. This representation indicates that water in mainly of the Bicarbonate –Sodium (HCO_3^-/Na^+) type in the central and marine portion of the sand bar, indicating a marine influence on groundwater salinity. The lagoon area can be classified (Rosado de Palacio, 2012) as a Chloride – Sodium (Cl^-/Na^+) type, indicative of the high salinity in that area. In the

eastern portion of the sand bar, the water is high in Magnesium ($HCO3^-/Mg^+$; Cl-/Mg+ and $SO4^-/Mg^+$), indicating influence of pesticides and fertilizers (Rosado de Palacio, 2012).
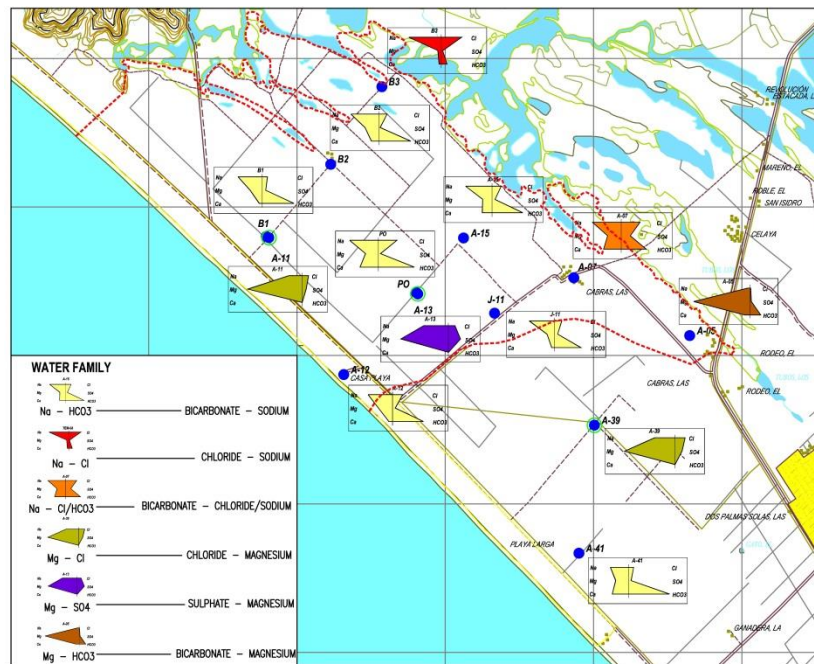
Figure 12. Distribution of Stiff diagrams and water families in the area of *Las Cabras*. Rosado de Palacio, 2012.

III. Theoretical Background of Numerical Model

One of the techniques used in numerical modelling to solve the groundwater flow equation is to use finite difference flow or finite element numerical methods by converting the partial differential equation into an algebraic approximation. These methods divide space and time into discrete intervals (finite cells) and solve the flow equation for hydraulic head for each cell; this is called the discretization mesh (Oberdorfer, 2003), as shown in Figure 13 below. Because this equation has no particular solution, the use of computers and numerical algorithms allows to generate, since the 1970's (Thiery, 2004), computer codes that simulate seawater intrusion for specific cases and characteristics of aquifer geometry in one, two and three dimensions (Sanford & Pope, 2010).
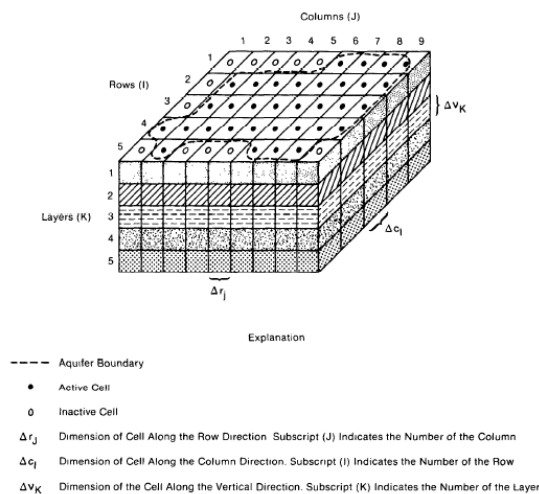
Figure 13. A discretized mesh representing a hypothetical aquifer system. From McDonalnd & Harbaugh, 1988.

For the numerical modelling of coastal aquifers, where saltwater intrusion occurs, in addition to solving the variable-density groundwater flow equation, the modelling can include solutions to the solute transport equation that solves for the migration of dissolved species (e.g. MOCDENS3D, SEAWAT). With the addition of an equation of state, which converts the concentration of solutes (usually TDS) to fluid density, thus making it possible to simulate the density-dependent flow interactions that occur when both fresh and seawater are present (Oberdorfer, 2003; Oude Essink, 2001).

In density dependent groundwater flow, such as that which occurs in coastal aquifers, the physical and chemical processes that occur in the mixing and flow of groundwater are related and dependent on each other. These processes are changes affecting the fluid density, which in turn is related to total dissolved solids (TDS) in groundwater. There are several mathematical formulations to represent these relations (equations of state), however, for simplicity in numerical modelling; the pressure and temperature changes are commonly disregarded and only density as a function of salinity is taken into account.

A linear form of the equation of state, relating chloride and density is given by:

$$\rho(C) = \rho_f \left(1 + \alpha \frac{C}{C_s} \right)$$
(1)

where $\rho(C)$ is the groundwater density at a given chloride concentration C, $\rho_f = 1000 \text{ kg/m}^3$ is the density of freshwater, $C_s = 19{,}000 \text{ mgCl}^-/\text{l}$ the chloride concentration of seawater and $\alpha = (\rho_s - \rho_f)/\rho_f = (1025 - 1000)/1000 = 0.025 \; [-]$ the relative density difference. Chloride is a conservative and non-reactive ion that is often used in explaining water salinity.

The equation of motion, which describes fluid flow in porous media and accounts for density differences, is given by Bear (1972):

$$\bar{q} = -\frac{\kappa}{\mu} (\nabla P - \rho \bar{g})$$
(2)

The components derived from equation (2) that represent flow in three dimensions are given by:

$$q_x = -\frac{\kappa}{\mu} \frac{\partial P}{\partial x} \qquad q_y = -\frac{\kappa}{\mu} \frac{\partial P}{\partial y} \qquad q_z = -\frac{\kappa}{\mu} \left(\frac{\partial P}{\partial x} + \rho g \right)$$
(3)

where q_x, q_y, q_z in m/d, is the specific discharge in the three principal directions; κ in m^2, is intrinsic permeability; μ in $kg/m/d$, is dynamic viscosity of groundwater, P in $[kg/m/d^2]$, is fluid pressure, ρ in kg/m^3 is fluid density and g in $[m/d^2]$, is acceleration of gravity.

Density dependent groundwater flow can be represented mathematically in terms of pressure (P) and density (ρ). However, since piezometric level(s) (h) are more intuitively understood and commonly used by hydrogeologists in the field, a mathematical relation can be assumed between P and h, given that a reference density is used (usually that of freshwater) (Post et al., 2007). The assumption states that if a piezometer with fresh and salt water were to be replaced by an imaginary equivalent of freshwater, then the density would be equal for all measurements. This assumption simplifies the modelling because the solution of the groundwater flow equation can be cast in terms of head. This yields the freshwater head term, h_f, so commonly used in modelling, and used in MOCDENS3D:

$$h_f = \frac{P}{\rho_f g} + z$$
(4)

where z is the elevation of the piezometer screen $[m]$.

The term freshwater hydraulic conductivity is also introduced: $k_f = (\kappa \rho_f g)/\mu_f$, and assuming that dynamic viscosity variations are minimal and can be approximated to be constant (Verruijt, 1980; Bear & Verruijt, 1987 in Oude Essink, 2001). Additionally, in this study, $K_x = K_y \neq K_z$, where K_x and K_y are the horizontal and vertical hydraulic conductivities, respectively and considering that no distinction is made between conductivity K and freshwater conductivity K_f, which has a fixed density ρ_f. With this understanding, by solving (4) in terms of pressure and inserting it in the x and y components of (3) and differentiating, then we obtain:

$$q_x = -\frac{k_x}{\mu}\left(\frac{\partial}{\partial x}(h_f - z)\rho_f g\right) = -K_{f,h}\frac{\partial h_f}{\partial x}$$

(5)

$$q_y = -\frac{k_y}{\mu}\left(\frac{\partial}{\partial y}(h_f - z)\rho_f g\right) = -K_{f,h}\frac{\partial h_f}{\partial y}$$

(6)

The vertical flow component, which accounts for density differences, is given by:

$$q_z = -\frac{k_z}{\mu}\left(\frac{\partial}{\partial z}(h_f - z)\rho_f g + \rho g\right) = -K_{f,v}\left(\frac{\partial h_f}{\partial z} + \frac{\rho - \rho_f}{\rho_f}\right)$$

(7)

Equation (7) is used by several density dependent flow and transport numerical codes including MOCDENS3D and SEAWAT. Assuming hydrostatic pressure (no vertical flow), $q_z = 0$, the change in freshwater head, dh becomes with depth (e.g. sea boundary in this study $dh = -2 * 0.025 = 0.5$).

$$dh = -dz((1025 - 1000)/1000)$$

(8)

Equation (8) is used to calculate the change in freshwater heads in the vertical boundaries of the model domain.

The computer code applied for the numerical simulation of this study is MOCDENS3D, developed by Oude Essink (1998, 1999), which couples the MODFLOW (Harbaugh & McDonald, 1996) and MOC3D (Konikow et al., 1996) codes, allowing for the simulation of density differences in groundwater. Within the MOCDENS3D code, the MODFLOW module solves the groundwater flow equation with an adaptation for density differences, as presented in equation (7), in order to be able to model density dependent flow. This adaptation for density is done by inserting a buoyancy term $(\rho - \rho_f)/\rho_f$, which is responsible for the generation of freshwater lenses on top of higher salinity water (Oude Essink, 2001; Visser, 2012). In MOCDENS3D, the groundwater and solute transport equations will be solved in the centre of each model cell, which is known as Block Centred Flow.

The advection-dispersion equation is solved in two steps; advection is solved by the MOC3D module via particle tracking using the Method of Characteristics (MOC), followed by dispersion which is solved by a finite difference method (Visser, 2012). The advection-dispersion equation may also solve for adsorption and decay. However, the transport mechanisms that are modelled here are advection, diffusion and dispersion since chloride is used as representative of TDS. The simplified advection-dispersion equation, (e.g. in the x-direction) can thus be given by:

$$\frac{\partial C}{\partial t} = D_x \frac{\partial^2 C}{\partial x^2} - \frac{q_x}{n_e}\frac{\partial C}{\partial x}$$

(9)

where D_x in m^2/d, is the hydrodynamic dispersion coefficient in the x-direction, q is the specific discharge and n_e is the effective porosity.

Groundwater of different salinity can be classified with theoretical values of EC, TDS, Cl and density, as shown in Table 1 below. In this study, salinity results will be shown in terms of Cl concentration.

Table 1. Guideline approximate values of fresh, brackish and saline water. Integrated with data from Custodio & Llamas (1976) and Custodio & Bruggeman (1987), Hem (1985) and Oude Essink (2001). Note that this table should be used horizontally (the comparison between some parameters in the same water-salinity range is not consistent).

Parameter	Fresh water	Brackish – Saline water	Seawater	Brine/Hypersaline water
EC (µS/cm)	< 1000	1000 – 10,000	54,000	> 54,000
TDS (mg/L)	0 – 1000	1000 – 10,000	35,000	> 35,000
Cl (mg/L)	0 – 300	300 – 10,000	19,000 – 25,000	> 20,000
Density (kg/m^3)	1000	1010	1025	1200 – 1300

Chloride can be related with TDS as follows (Hiscock, 2005):

$$TDS \; (mg \; L^{-1}) = \; k_e \cdot EC \; (\mu S \; cm^{-1})$$

(10)

where the correlation factor k_e generally has values of 0.5 and 0.8.

IV. Model set-up

This section describes the methodology used in building the model, including the geometry and design of the grid, the temporal discretisation, the boundary and initial conditions, the model packages used as input files and the resulting scenarios and reference case where limited calibration was done. A conceptual representation of the model set-up and parameters is presented in Figure 14. Table 2 provides an overview of the parameters and properties. The model was constructed as a 2D aquifer slice mainly for two reasons: one is to make it as simple as possible, considering only the major processes that determine the flow and mixing of groundwater; and two is due to the limitation of data on a large scale in the area.

Processing Modflow (PMWIN), developed by Simcore Software, was used for the initial creation of model geometries and input files (model packages) and was later partially replaced by Pascal programming scripts. Tecplot, developed by Amtec Engineering, is used to display the output of heads, concentration configurations, velocity fields, streamlines and animations.
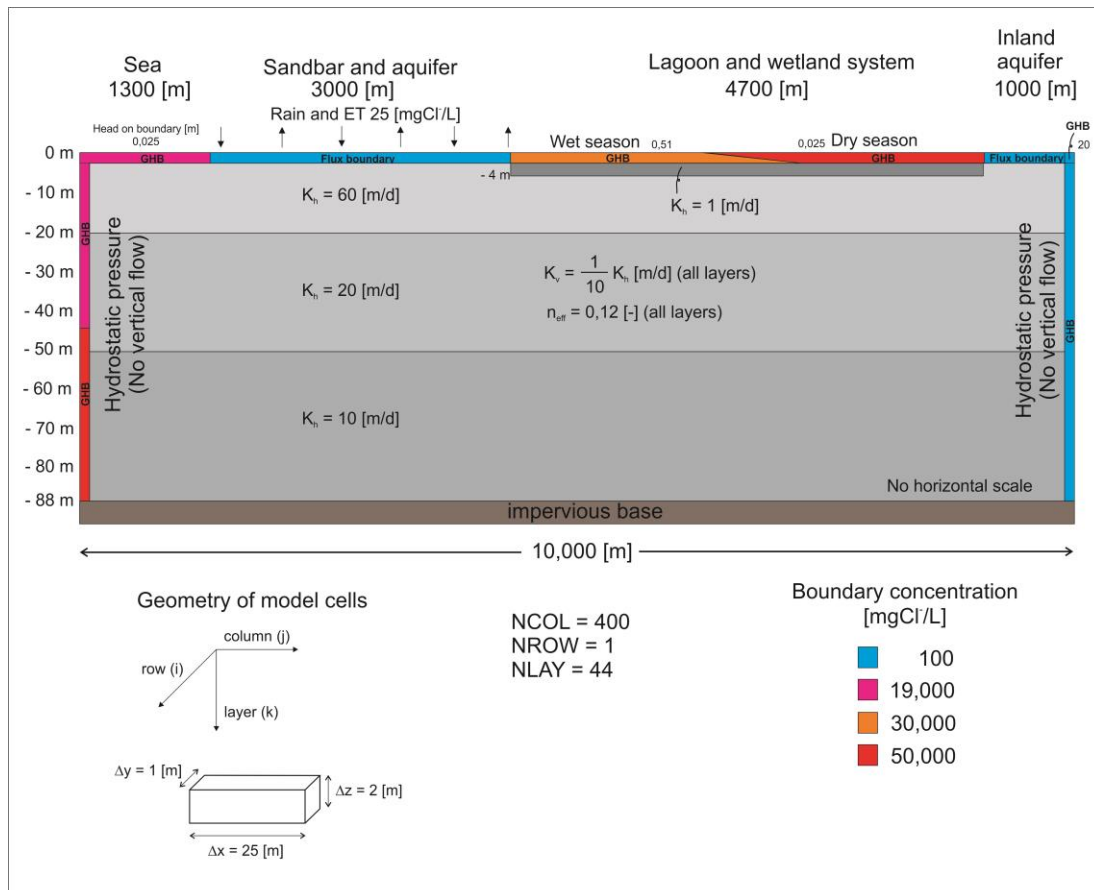
Figure 14. Geometry and parameters of the numerical model.

Geometry and grid design

Several considerations were taken into account when selecting the geometry and grid design of the model. The horizontal extent had to be long enough to include the sea, sand bar, lagoon system and a portion of land that simulates the inland aquifer. Therefore an extent of 10,000 m was deemed sufficient. The spatial discretisation comprises 400 columns in the horizontal direction and 44 layers in the vertical direction. The spacing between layers is set as 2 m for all layers, thus the vertical depth of the model corresponds to the depth assumed to be the bedrock in the study area. All layer types are set as confined, where $T = kD = $ constant.

Temporal discretisation

Seasonal variations of wet and dry periods seem to have a major influence on the freshwater lens. Therefore these seasonal periods were modelled in the *Basic* (*Bas*) package in two stress periods per year. The wet period has a rough duration of 4 months = 121.75 d (July – October) followed by the dry period of roughly 8 months = 243.5 d (November – June). Each stress period is divided into 100 time steps, therefore yielding time steps of 1.22 d and 2.44 d respectively. This means that new heads and concentrations are computed for every time step in each model cell. These small time steps help reduce numerical errors during the simulation (Oude Essink, 2000). The total simulated time is 500 years.

Boundary conditions

Two boundary types are used in this model, the *General Head Boundary Package* (GHB) and a flux boundary. For the GHB package, in each cell, the head is calculated within the model domain. However, the GHB package overrides variable heads in the cells where it is enforced (Oude Essink,

2014, personal communication). To make this happen, the conductance of the GHB cells is set to 100 m^2/d. The sand bar has a flux boundary, being dependent on recharge and evapotranspiration via the *Wel* package.

The top of the model does not represent the topography, but is instead a representation of groundwater head. Therefore, any changes in inflow or outflow in the top boundary occur directly on the simulated water table. The top boundary conditions were set as GHB in the sea, lagoon and top right corner cell and prescribed equivalent freshwater heads and chloride concentrations of 19,000 $mgCl^-$/L, 30,000 $mgCl^-$/L and 50,000 $mgCl^-$/L (for wet and dry periods) and 100 $mgCl^-$/L respectively at each segment (Figure 14). The freshwater heads for each segment are 0.025 m, 0.51 m and 0.025 m (for wet and dry periods) and 20 m respectively. The sand bar and inland aquifer were set as flux boundaries, the former being dependent on recharge and evapotranspiration via de *Wel* package and the latter being influenced by the top right corner cell. The left and right vertical boundaries were set as GHB from layers 2 to 44. The prescribed freshwater heads start acting from the top boundary. This occurs as explained in equations 4-8 above, with a freshwater head that increases with depth. On the sea side, the concentration from 0 m to –44 m is set to 19,000 $mgCl^-$/L and from –46 m to –88 m it is set to 50,000 $mgCl^-$/L. This interval of higher concentration, from –46 m to –88 m, allows the "outflow" of brine coming from the lagoon portion of the model and was assigned at this depth due to observations in model runs where the brine plume reached an approximate depth of –46 m to –88 m in the left vertical boundary (see scenarios 1-5 in Annex 1). The inland aquifer vertical boundary concentration is set as 100 $mgCl^-$/L. This boundary is based on two assumptions: 1) on the inland side only freshwater enters the aquifer which is plausible as base flow coming from the mountains and, 2) given the topographic elevation, groundwater head will be relatively constant and higher than in the coastal plain. The bottom boundary at –88 m.b.s.l is considered as a no-flow boundary.

The model boundaries are placed more than 500 m from the sand bar and lagoon systems to reduce numerical conceptual errors introduced by the boundaries.

Initial conditions

The purpose of the reference case is to arrive at the field measured situation of the freshwater lens and the assumed salinity distribution between the fresh, saline and brine water. To achieve this, a uniform salt domain is set at 19,000 $mgCl^-$/L and the model is run until the freshwater lens forms and the system arrives at an apparent equilibrium. Model units are metres and days. Groundwater heads are modelled as the dynamic cyclic steady state condition, where the head varies in space and time, e.g. due to seasonal recharge rates (Oude Essink, 2000).

Hydrogeological parameters and stresses

The selection of hydrogeological parameters is based on the geological, geophysical and hydrogeological information of Rosado de Palacio (2012). Given that relatively detailed information of the subsurface is only available in the area of the sand bar, the parameters for this area were extrapolated to the entire model domain. Thus, hydraulic conductivity is separated into three zones. The top zone is found between 0 m and –20 m, characterized by medium to fine sand, and is given a horizontal hydraulic conductivity of 60 m/d. The mid zone is found from –20 m to –50 m, also composed of medium sand but with a higher content of clay and silt, therefore an approximate value of 20 m/d is given for this zone. The bottom zone is found from –50 m to –88 m, also composed of medium sand with some clay and loam lenses, a hydraulic conductivity of 10 m/d was assigned to this zone. In the area of the lagoon system, a horizontal hydraulic conductivity of 1 m/d was assigned in the first 4 m due to the high clay and loam content observed in field visits in Rosado de Palacio (2012). Considering that the geological materials are sedimentary in origin and the effect of compaction increases with depth, vertical hydraulic conductivity is taken as one order of magnitude lower than its horizontal component. Effective porosity is given a value of 0.12 [–] for all layers. This apparently small value, obtained during the pumping test in Rosado de Palacio (2012), was changed to higher

values in some model runs (see Annex 1). However, it did not seem to have a major effect in the size and shape of the freshwater lens and overall concentration distribution.

For the seasonal groundwater head variation in the freshwater lens, rain and evapotranspiration seem to be the major players and are therefore modelled as occurring only in that area. The *Wel* package is used for this purpose and incorporates recharge and evapotranspiration values in a consistent way.

Model packages

The MODFLOW code is composed of the main program and several independent subroutines called modules, these modules are grouped into packages, which simulate a particular aspect of the hydrogeological system (McDonald & Harbaugh, 1988). The main model packages incorporated into this model are the *Basic* (*Bas*), *Block-Centered Flow* (*Bcf*), *Preconditioned Conjugate Gradient 2* (*Pcg2*), *Mocmain, Wel, General Head Boundary* (*GHB*) and *Densin.dat* packages. These packages are manipulated via input files where parameters are assigned and are then incorporated by the model.

The *Bas* package contains geometrical and temporal model data, including the number of layers, rows, columns, stress periods, time steps and length of time steps. It also includes the IBOUND array and an initial starting head configuration at the beginning of the simulation. The *Bcf* package numerically calculates flow within the porous medium, gives permeability values to model cells and specifies either steady state or transient flow. The *Pcg2* package gives the numerical parameters for solving the equations for hydraulic head. The *Mocmain* package is similar to the MOC3D package, here adapted for MOCDENS3D, it includes data of physical and chemical transport parameters such as concentration, dispersion values and porosity. The *Wel* package is used to simulate recharge and evapotranspiration, where inflow (+) and outflow (-) values are given for every stress period on the top boundary row where the sandbar is modelled. The *GHB* package functions as a head dependent boundary condition, where inflow or outflow from a GHB cell varies in proportion to a simulated head that is assigned as a constant head in an external fictional source. From this external source, a head on the GHB cell is obtained via a proportionally constant value of hydraulic conductance, between the GHB cell and the external source. The *Densin.dat* package accounts for the Equation of State for density differences and buoyancy and assigns colours to the output displayed in an animation.

Calibration

The limited calibration for this model was done manually via trial and error, using the field data as a reference case, running the model and comparing the output to measured field data such as salinity profiles and groundwater head measurements. From this comparison, adjustments were made to one or more of the trial parameters until the measured and computed output had a better fit. The model runs were done in steady state for each stress period where hydraulic heads reach equilibrium after each time step.

Table 2. Model parameters and values.

Model parameter	Value
Model area	0.88 km^2
Horizontal cell size	25 m
Horizontal model extent	10,000 m
Number of cells (all active)	17,600
Bottom of model domain	–88 m.b.s.l
Stress period length (seasonal)	4 months (wet), 8 months (dry)
Number of time steps	100
Effective molecular diffusion coefficient	8.64 x 10^{-5} m^2/d
Courant number	4 [–]
Longitudinal dispersivity	0.2 m
Horizontal transverse dispersivity	0.02 m
Vertical transverse dispersivity	0.02 m
Hydraulic conductance (GHB cells)	100 m^2/d
Recharge rate (including return irrigations)	400 mm/yr (Rosado de Palacio, 2012)
Evapotranspiration rate	379 mm/yr (Rosado de Palacio, 2012)
Pumping rate	30 mm/yr (Rosado de Palacio, 2012)
Rain concentration	25 mgCl$^-$/L
Seawater concentration	19,000 mgCl$^-$/L
Brine concentration (seasonal)	30,000 mgCl$^-$/L (wet), 50,000 mgCl$^-$/L (dry)
Horizontal hydraulic conductivity (zone)	60 m/d (top), 20 m/d (mid), 10 m/d (bottom)
Vertical hydraulic conductivity (zone)	6 m/d (top), 2 m/d (mid), 1 m/d (bottom)
Anisotropy K_v/K_h	0.10
Effective porosity	0.12 [–] all layers

V. Results and discussion

Arriving at reference case

Once all parameters have been set and assigned in the input files. The model was run for 500 years. In all scenarios, the thickness of the fresh water lens is defined at the iso-salinity contour of 300 mgCl$^-$/L for freshwater and 10,000 mgCl$^-$/L for brackish-saline water with any values above the latter considered as saline. The iso-salinity contour of brine is established at ≥ 20,000 mgCl$^-$/L.

Many model runs were carried out, varying certain parameters (see Annex 1). These parameters include: the K_v and K_h, the effective porosity, the volume of freshwater entering and leaving the system in the *Wel* package, the number of wells that simulate rain and evapotranspiration and their position (in all cells of the top boundary or only in the top cells of the freshwater lens), the fixed concentration in the GHB left vertical boundary and the initial freshwater head in the lagoon during the wet season. Of all these scenarios, the one that has a closer fit to the field situation was selected. For the selection of this scenario or reference case, the considerations that were taken into account are: 1) the size, shape and concentration of the freshwater lens directly related to the values given in the *Wel* input file, 2) the initial head in the right side inland aquifer boundary cell, 3) the horizontal hydraulic conductivity, 4) the initial and seasonal prescribed heads and concentrations in the GHB boundaries, 5) the effective porosity. A table with selected scenarios and a summary of their input files is presented in Annex 1.

Since the seasonality of the freshwater lens is of such importance for arriving at the reference case, it is modelled with three approaches. Scenario 1 is taking the measured rainfall and evapotranspiration values of the *La Concha* weather station averaged over the wet and dry periods, from 1968-2008 as a loop of 38 years (some years lack measurements) that repeats until the end of the model run of 500 years. Scenario 2 is taking rainfall and evapotranspiration values from the *La Concha* weather station for a reference year and using both values as a loop that repeats until the end of the model run of 500 years. The year 2004 is selected due to the completeness of the data and additionally because the average yearly values for both events (rainfall and evapotranspiration)

resemble the average values of the measurement period (1961-2008). Scenario 3 is taking the recharge, evapotranspiration and pumping rates from Table 2 which are given in Rosado de Palacio (2012). Evapotranspiration and pumping are added together as sinks and recharge as source, both values are used as a loop that repeats until the end of the model run of 500 years. The resulting scenarios are presented below in Figure 15. These are considered to be the closest approximations to the field measured situation.
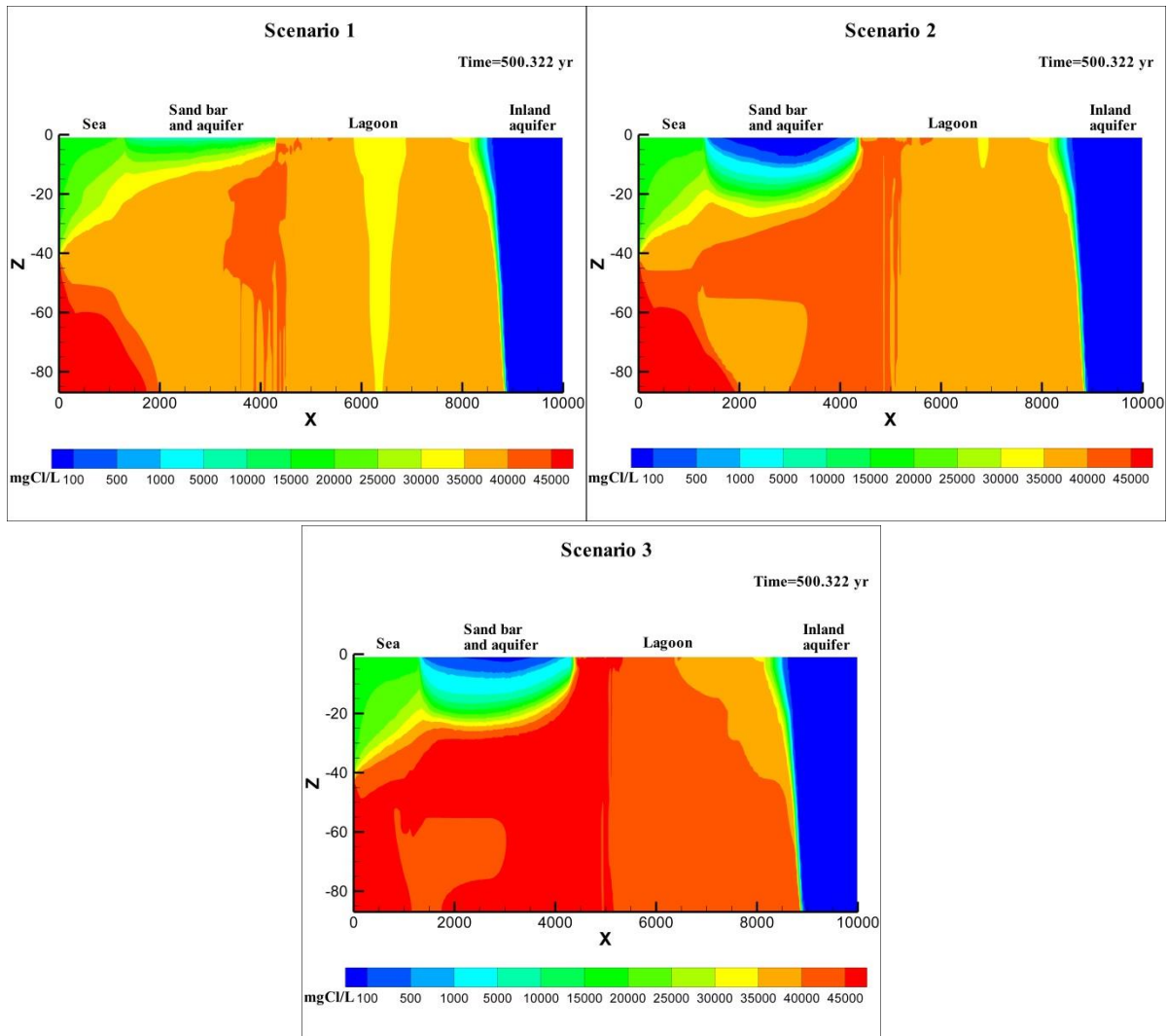
Figure 15. Scenarios used to arrive at reference case.

From the resulting concentration configurations, scenarios 1 and 2 produce a freshwater lens that is either too thin or too deep, respectively. In scenario 1, a freshwater lens never forms, with lowest concentrations ranging between 6,000 and 10,000 mgCl⁻/L in the first 2 m.b.s.l in the sand bar. In scenario 2, the freshwater interface extends to approximately –9 m.b.s.l and seawater concentration is found at approximately –20 m.b.s.l. This is a closer approximation to the field situation but the freshwater lens and the mixing zone are still too deep. In both scenarios, the brine plume that forms in the left boundary is of higher concentration than the plume that comes from the lagoon boundary. Scenario 3 is the closest approximation to the field measured situation in the concentration distribution of the freshwater lens. It is therefore selected as reference case.

Reference case

The reference case is assumed to be a closer representation of the actual field situation. In this case, given enough time, the freshwater lens forms distinctly separated from surrounding saline water bodies. It begins to form after approximately 20 years of rain and continues to grow until after approximately 100 years. It then continues to expand and contract according to the wet and dry seasons until the end of the simulation. At this time, the freshwater interface reaches a depth of –5 m.b.s.l in the thickest portion of the lens in the wet season and during the dry season it reaches a depth of –3.5 m.b.s.l. The variation of the freshwater interface is therefore about 1.5 m between seasons. It is underlain by a gradual mixing zone found at –20 m.b.s.l in the centre of the sand bar, at –15 m.b.s.l in the sea boundary and at –6 m.b.s.l in the lagoon boundary. This concentration configuration is similar to the conceptual model of Figure 11. However, the dilution of salinity that is observed in the salinity profiles in Figure 10 at a depth between –40 m and –55 m is not observed in this reference case. In this reference case, the brine plume underlying the freshwater lens does not reduce in concentration during the wet season

In the lagoon boundary, brine pockets initially descend into saline groundwater in the contact zone between the freshwater lens and the lagoon. Density differences are highest in this area initially forming salt fingers and a mixing zone is produced due to hydrodynamic dispersion. The formation of these fingers starts to occur after the second stress period. Already after approximately 4 years, these saline fingers reach the bottom layer of the model, thus evidencing a very quick process. Then, after approximately 10 years, fingering starts to occur in the right side of the lagoon. Within 20 years, the saline fingers on the left side start to be density driven towards the left boundary and after 60 years these fingers now encompass the entire horizontal extent of the lagoon boundary and the entire section underlying the lagoon is highly saline. Around this time, the brine plume coming from the lagoon begins to mix with the brine plume coming from the left boundary. Note that this steady state artificial boundary condition is set to make a proper consistent boundary condition with outflowing brine. If this condition is not set, then the boundary condition gives an unrealistic concentration at this boundary (see Annex scenarios 1 to 5). After 180 years, the entire section underlying the freshwater lens has a brine concentration of >30,000 mgCl$^-$/L. Following this time, brine continues to displace the lower salinity water and after 250 years, most of the model domain is completely dominated by high density brine. In the remaining 250 years, concentration continues to increase and to displace lower salinity brine towards both the left and right boundaries. On the left vertical boundary, brine with a concentration of 50,000 mgCl$^-$/L flows into the system until approximately 150 years, when the flow begins to change direction, first flowing upwards and then after 170 years the flow is directed outside of the system, towards the left vertical boundary. Following this time, brine continues to flow out of the system. Images of these changes are presented in Figure 16 and 18 below.

The right boundary remains fresh, as a column of freshwater, due to the relatively high (20 m) groundwater head which is maintained constant at the right boundary throughout the simulation. On this boundary, the freshwater head is high enough to keep the brine plume at bay.

The vector size in the simulation is set to 500 relative units (Grid units/magnitude) to illustrate the flow direction and its relative magnitude. From the vector field, it is evident that the right side boundary has a constant and major effect on the concentration and head distribution in the system since it is here that groundwater heads and flow velocities are highest. The inflow and outflow in the sand bar is also represented by vectors that are entering or leaving the system. It is important to note that the inflow and outflow direction influences the velocity field until at least –40 m.b.s.l, which is an indication that the processes (rain and evapotranspiration) that occur on the surface of the aquifer have a significant effect on the flow in the lower layers (see detail in Figure 16 **c** and **d**). This is probably due to the steady state simulation, where sudden changes can theoretically affect a water system at infinite distance or depth. The vector field also shows the constant brine in-flow into the system in the lagoon boundary, particularly in the zone where the lagoon is in proximity to the freshwater lens. The fact that it is more pronounced on the side of the freshwater lens can be due to the fact that the constant head assigned on the right side corner cell prevents higher vertical flow vectors on the right side of the lagoon system.

Figure 16 **a** and **b** shows the concentration distribution in the last two stress periods at the end of the simulation. The major significant difference between them is the inflow and outflow direction in the freshwater lens corresponding to the wet and dry seasons. Additionally, the vertical flow at either side of the sand bar is higher during the dry season, this can be due to the fact that during the wet season there is freshwater flowing into the system in the freshwater lens, thus creating a convective flow zone below it that decreases the flow magnitude of saline water in-flowing at either side of the freshwater lens. With a zoom in the freshwater lens in **c** and **d**, it is possible to view in greater detail the direction of flow in the wet and dry seasons, and the influence that the inflow and outflow (which are modelled in the top layer only) has on deeper layers. Note also the rotational vectors in the contact between high and low concentrations.
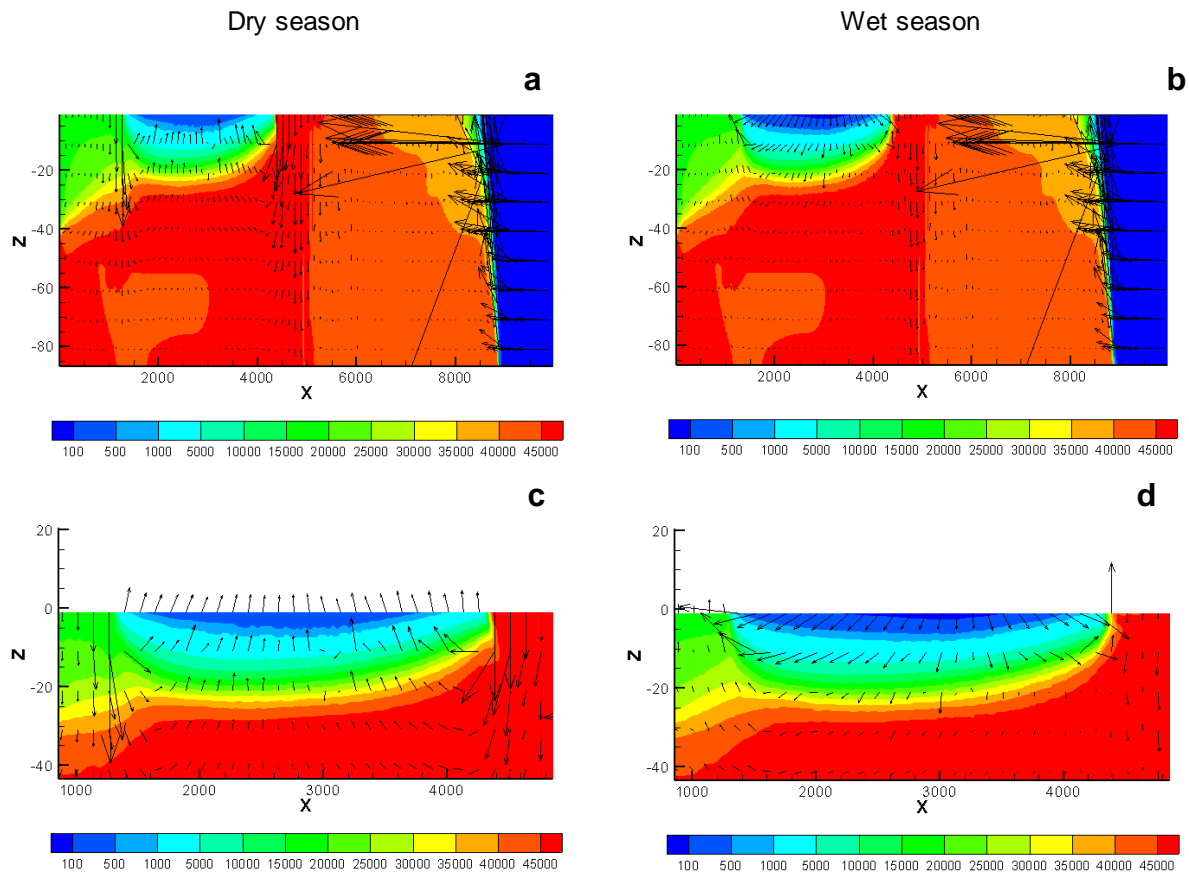
Figure 16. Concentration distribution and velocity field in the last two stress periods of the simulation (t=500 yr). **a** and **b** shows the entire system and **c** and **d** shows a zoom of the area of the freshwater lens. The units of the horizontal and vertical axes are metres and concentration units are $mgCl^-/L$.

The freshwater head distribution is displayed in Figure 17 below. Only the last two stress periods are shown, with the resulting configuration of the freshwater heads and the influence of the seasons on the entire system. Streamtraces and markers (yellow squares that represent actual particles) are plotted with each figure to show the direction of flow of water and chloride particles. A delta time (the space between markers) of 10 years is set for the display of markers. This shows that the density of particles is, as expected, highest in the section underlying the lagoon and also that the space between particles decreases with depth, which is especially visible during the wet season in the area underlying the freshwater lens. The freshwater head increases with depth as explained in equation (7) due to density differences where flow is occurring from zones of high concentration to low concentration and from zones of high freshwater head to low freshwater head. Note the fixed head on the right side boundary. During the dry season, particles flow from the sea and lagoon towards the freshwater lens and from the lagoon towards the right side boundary. This can be due to the steady state simulation and the extended vertical influence of rain and evapotranspiration in the top

horizontal boundary. During the wet season, particles flow radially from the freshwater lens to the sea and lagoon, some leaving the system on the left vertical boundary. In the lagoon they flow towards the right side boundary in tortuous paths which resemble the fingering process that was visible in the initial stress periods of the simulation. During both seasons, particles flow from the right side boundary towards the lagoon, given the relatively high constant freshwater head on the vertical right side boundary. This evidences that a high constant freshwater head can keep high salinity (e.g. brine) at bay.

Table 3 shows the values of the freshwater head in different parts of the lens during the wet and dry seasons.

Table 3. Modelled vs. measured freshwater head fluctuations in the top of the freshwater lens. Measured groundwater heads are taken from Figure 8.

	Wet season (m.a.s.l)	Dry season (m.a.s.l)	Variation between seasons (m)
Modelled			
Centre	1.41	–0.18	1.23
Sea coast	0.54	0	0.54
Lagoon	1.04	0.04	1.00
Measured			
Centre	2.00	1.25	0.75
Sea coast	1.90	1.40	0.50
Lagoon	1.60	0.95	0.65

From measurements in Rosado de Palacio, (2012) and from Figure 8, measured seasonal groundwater head differences in the sand bar are variable: in the centre of the sand bar, where the bulge of the freshwater lens is highest (Figure 7a and 7b), the variation is approximately 0.60 m between seasons; closer to the sea boundary it fluctuates between 0.20 m and 0.60 m in zones with no pumping and 1 m in zones with pumping; and in the lagoon boundary it varies between 0.30 m and 0.80 m. Modelled head variations are a close approximation to measured values. Nevertheless, in the model, the actual head elevations are underestimated. This is likely due to the steady state simulation and perhaps to the 2D approach. A transient simulation incorporating storativity may have produced a closer match between modelled and measured heads. However, the interest of this study was on long term changes to the system.
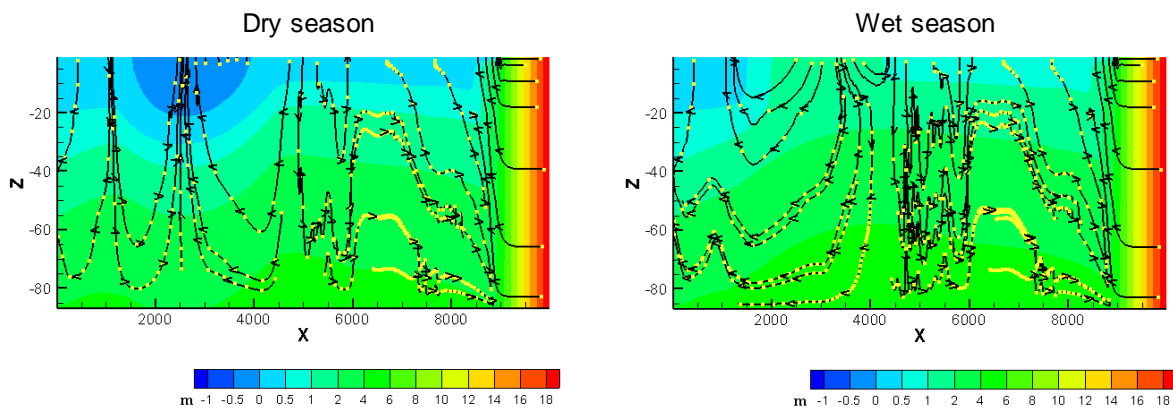

Figure 17. Seasonal freshwater head configuration at the end of the model simulation (t=500 yr). The units of the horizontal and vertical axes are metres.
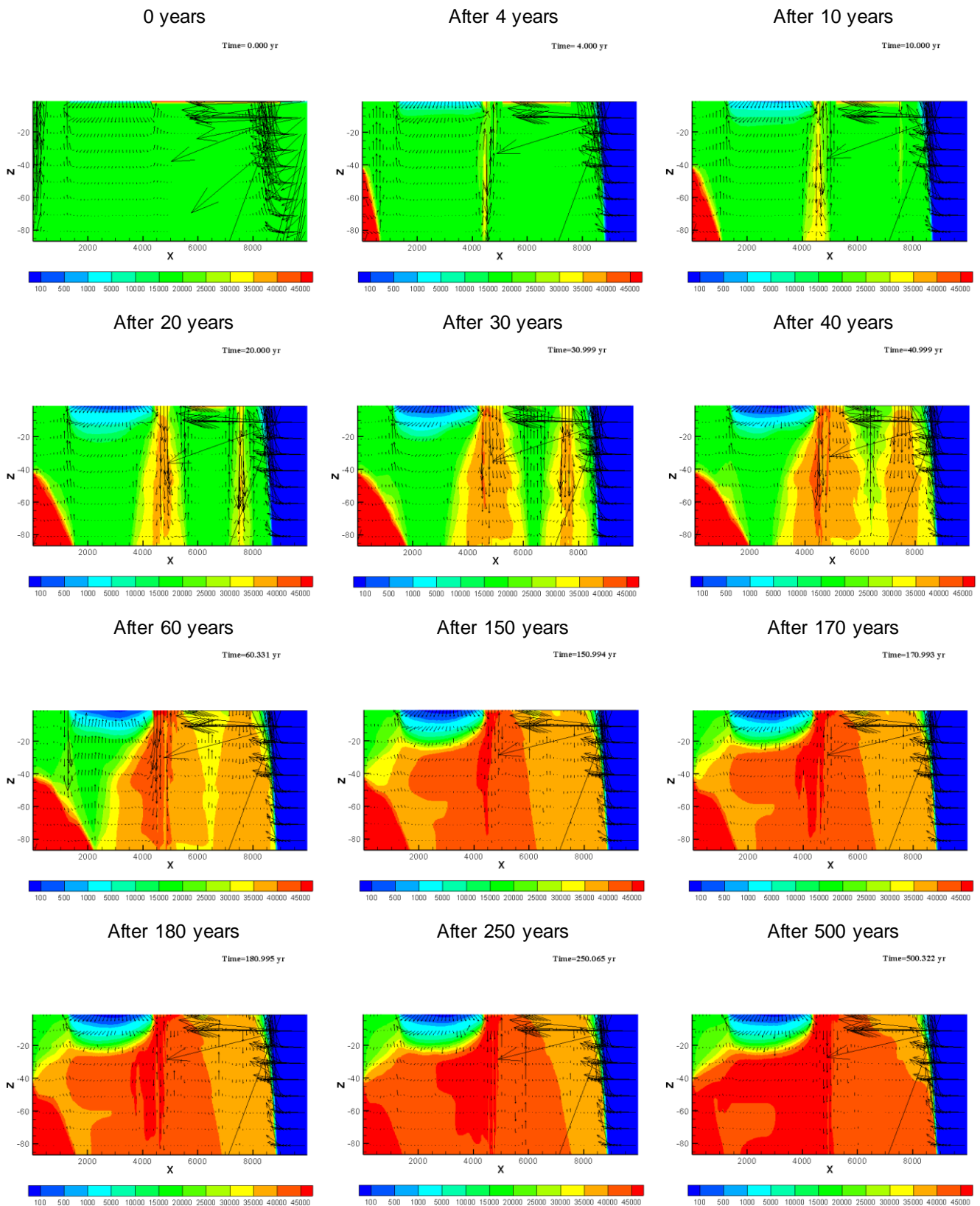
Figure 18. The evolution of the concentration distribution in the system in the reference case. The units of the horizontal and vertical axes are metres and concentration units are mgCl⁻/L.

Future scenarios

Three scenarios of future climatic changes were modelled: A) Sea level rise of 0.85 m by 2081-2100 relative to 1986-2005 according to the RCP8.5 projection on the IPCC fifth assessment report (IPCC, 2013). B) Longer periods of drought, modelled as a 20% increase in evapotranspiration and C) Combined sea level rise and drought.

A) Rising sea level due to climate change

The RCP8.5 projection predicts a likely global mean sea level rise range of between 0.45 m and 0.80 m in 2081-2100 relative to 1986-2005 (IPCC, 2013). The highest sea level change of 0.80 m was chosen to show the effect of such a scenario in the freshwater lens and in the entire system. For this simulation, the only parameter that was changed is the initial freshwater head in the top horizontal GHB sea boundary, in order that by the end of the model run of 500 years, the freshwater head gradually increased from 0.025 m to 0.80 m. The resulting configurations are shown in Figure 19.

From the model results, hydraulic heads increase in the freshwater lens due to sea level rise (Table 4). The difference in hydraulic heads is highest in the sea coast and they decrease gradually towards the lagoon. Modelling results of Oude Essink et al. (2010) for sea level rise in the Netherlands also show increasing hydraulic heads in a 10 km zone of influence from the coastline.
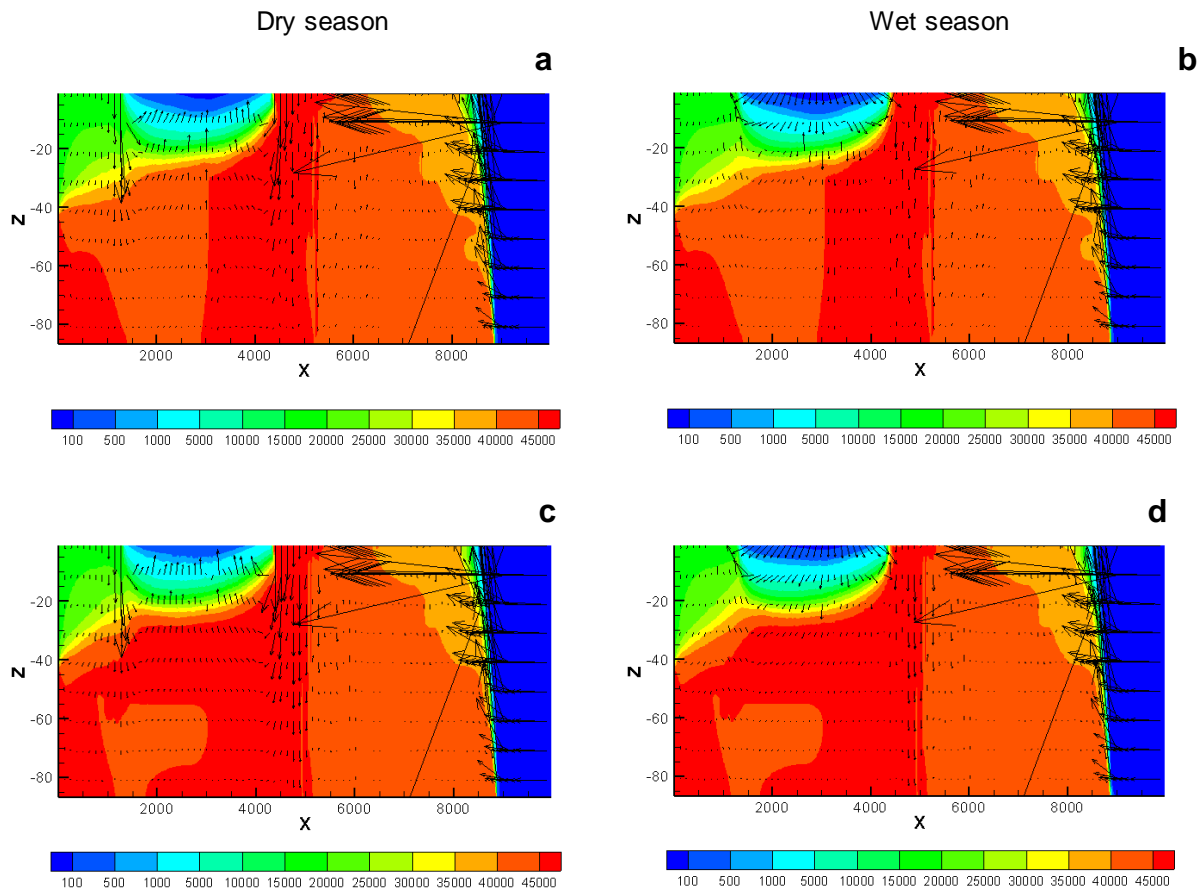
Figure 19. **a** and **b**. Resulting concentration distribution with 0.80 m of sea level rise by 2081-2100. **c** and **d** are the dry and wet seasons of the reference case for comparison. The units of the horizontal and vertical axes are metres and concentration units are mgCl⁻/L.

In the concentration distribution, the higher freshwater heads in the freshwater lens produce lower concentrations and a thicker freshwater lens. The iso-salinity contour of 300 mgCl-/L now extends to –7 m.b.s.l in the centre of the sand bar during the wet season and to –6 m.b.s.l during the dry season, which represents more than 2 m difference from the reference case. This could be due to the higher

freshwater heads induced by sea level rise, where the brine is pushed downwards enabling the formation of a thicker freshwater lens.

B) Longer periods of drought with a 15% reduction in precipitation and 15% increase in evapotranspiration

For this scenario, longer periods of drought are simulated with a decrease in precipitation and an increase in evapotranspiration via the *Wel* package. Temperature is predicted to increase, with a median of 3.2°C warmer by 2080-2099 in Central America including Mexico (Karmalkar et al. 2011, IPCC, 2007). For precipitation, several authors agree (Karmalkar et al. 2011, IPCC, 2007) that in Mexico it is projected to decrease over the next century, with varying magnitudes depending on the geographic location (Karmalkar et al. 2011). IPCC (2007) projections for Central America and Mexico predict changes in mean precipitation in the range of –48% to 9%. However, half the models predict changes between –16% to –5% (Christensen et al. 2007 *in* Karmalkar et al. 2011). Karmalkar et al. (2011) predict decreases in precipitation of between 0% and –24% in the geographical area of this study. For this scenario, a selected value of –15% in precipitation was chosen which is in close accordance with IPCC (2007) and in the range reported by Karmalkar et al. (2011). An evapotranspiration increase of +15% was selected considering the projected increase in median temperature. These changes were set to occur since the beginning of the simulation until the end of the model run of 500 years. The resulting configurations for this scenario are shown in Figure 20.
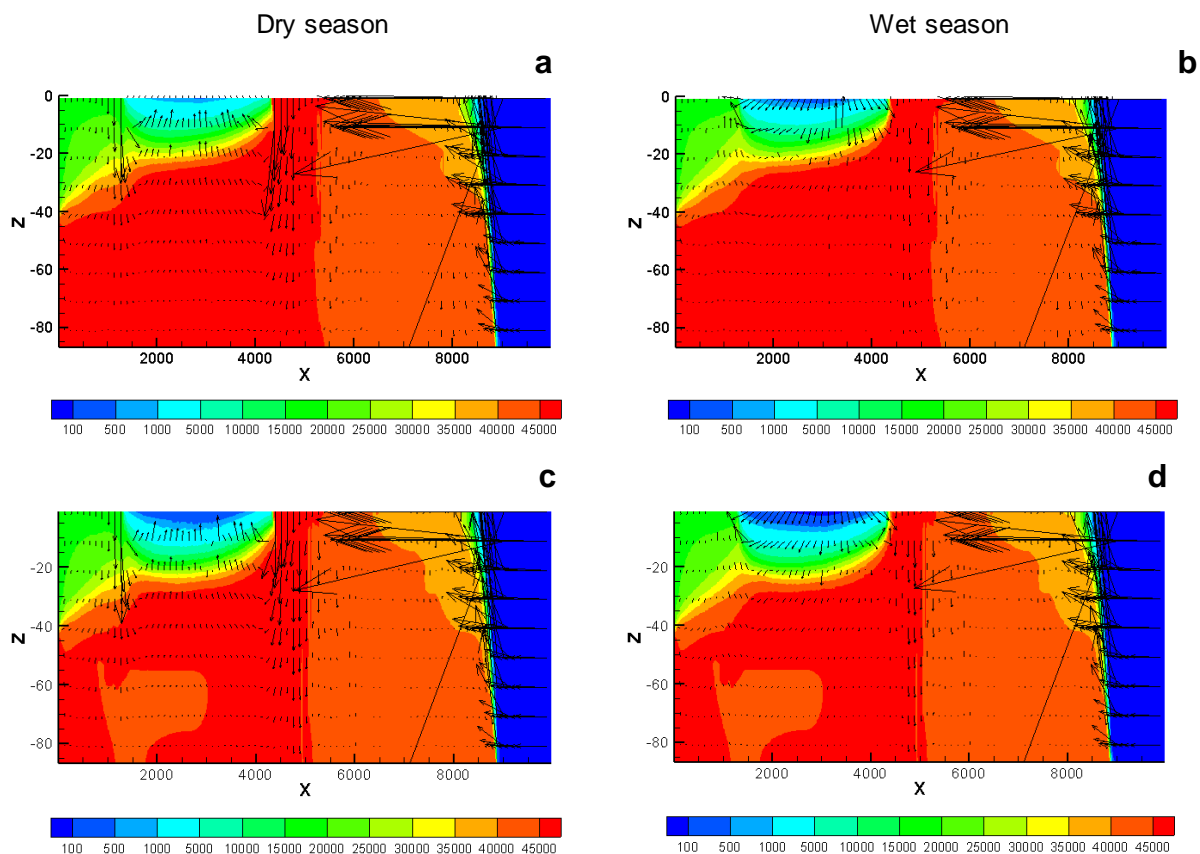
Figure 20. **a** and **b**. Resulting concentration distribution after a 15% decrease in precipitation and 15% increase in evapotranspiration in the freshwater lens . **c** and **d** are the dry and wet seasons of the reference case for comparison. The units of the horizontal and vertical axes are metres and concentration units are mgCl⁻/L.

The resulting configurations show, as expected, a lower freshwater head both in the wet and dry seasons compared to the reference case. From Table 4 it is evident that the change is more pronounced in the dry season. However, the greatest change occurs in the concentration distribution of the freshwater lens. The freshwater interface (300 mgCl⁻/L) in the centre of the sand bar is found at

–1.5 m.b.s.l in the wet season and during the dry season this interface disappears, with lowest values of 440 mgCl⁻/L in the top of the lens, which is roughly 3 m shallower than in the reference case. This result indicates the vulnerability of the freshwater lens to changing rain and evapotranspiration regimes. The flow velocity field shows a difference between the reference case and this scenario particularly in the boundary between the freshwater lens and the lagoon (Figure 20 **a**), with larger vectors entering the system in this area.

C) Combined sea level rise and drought

For this scenario, the combined effect of the preceding two scenarios was modelled. The hydraulic head results (Table 4) show a similar situation to scenario A), with higher seasonal freshwater heads compared to the reference case. This indicates that the effect of higher freshwater heads from sea level rise has a greater influence on the freshwater lens than the decrease in precipitation and increase in evapotranspiration. Nevertheless, the thickness of the freshwater lens is lower than in scenario A) and the reference case. In this case, the freshwater interface (300 mgCl⁻/L) in the centre of the sand bar extends to –3.5 m.b.s.l in the wet season and to –2.5 m.b.s.l in the dry season, which is 1.5 m thinner than the reference case in the wet season and 1 m thinner in the dry season. The resulting configurations are shown in Figure 21.
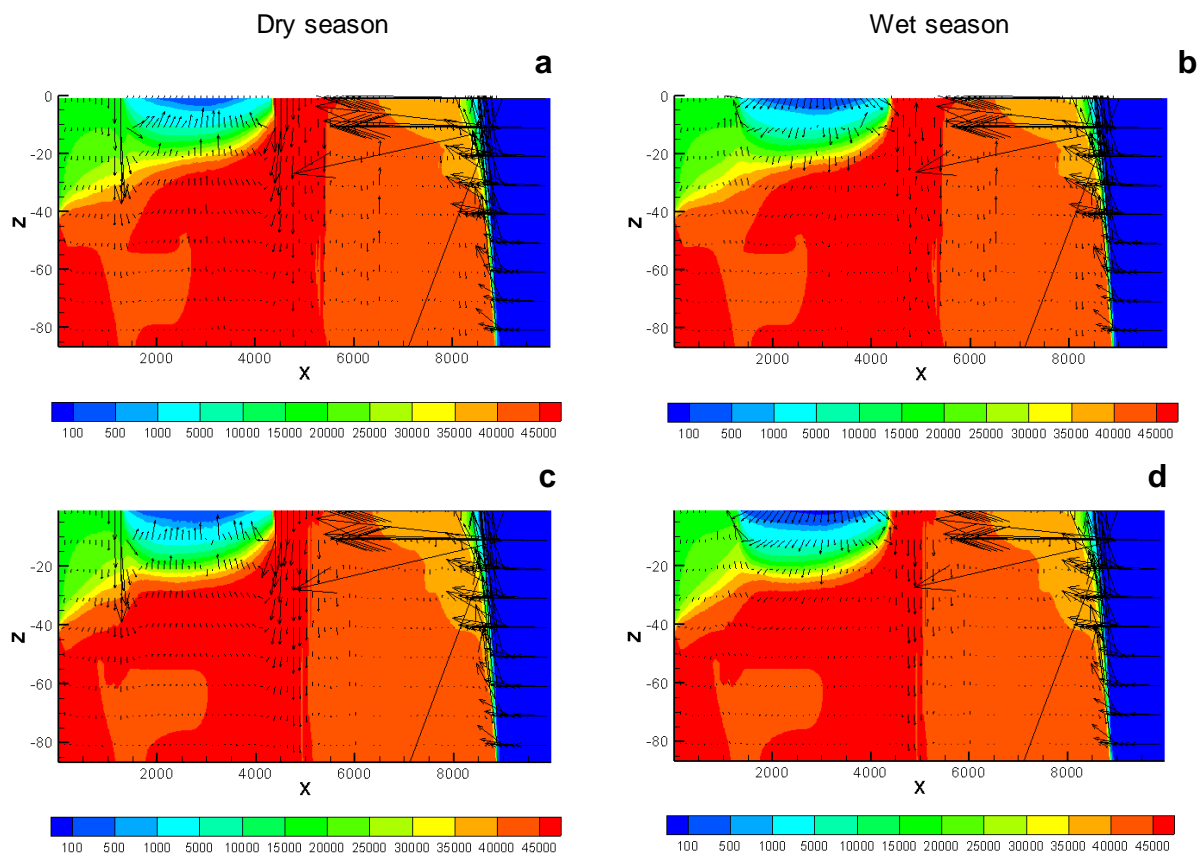
Figure 21. **a** and **b**. Resulting concentration distribution with 0.80 m of sea level rise by 2081-2100 and a 15% decrease in precipitation and 15% increase in evapotranspiration at the end of the model simulation (t=500 yr). **c** and **d** are the dry and wet seasons of the reference case for comparison. The units of the horizontal and vertical axes are metres and concentration units are mgCl⁻/L.

The concentration configurations do show (Figure 21 **a** and **b**) that the brine is pushed downwards as in scenario A), which is again evidence that the higher freshwater heads induced by sea level rise have an effect in the density distribution below the sea and freshwater lens boundaries.

28

Table 4. Modelled freshwater heads in different zones in the top of the freshwater lens for changing climatic conditions.

	Wet season (m.a.s.l)	Dry season (m.a.s.l)	Variation between seasons (m)
Reference case			
Sea coast	0.54	0	0.54
Centre	1.41	–0.18	1.23
Lagoon	1.04	0.04	1.00
Sea level rise			
Sea coast	1.23	0.72	0.51
Centre	1.85	0.26	1.59
Lagoon	1.16	0.15	1.01
Drought			
Sea coast	0.46	–0.08	0.38
Centre	1.24	–0.37	0.87
Lagoon	0.95	–0.11	0.84
Sea level rise & drought			
Sea coast	1.16	0.64	0.52
Centre	1.69	0.10	1.59
Lagoon	1.07	0.06	1.01

VI. Conclusions and recommendations

The main scope of this study was to better understand the hydrogeological system via the creation of a numerical model that would reproduce the hydrogeological behaviour of the coastal aquifer and surrounding saline water bodies. The modelling outcome in this work was useful to determine the main parameters that drive head and concentration changes in the coastal aquifer. The results of this work resemble the modelling outcomes of Kafri et al. (2013), who modelled two case studies where brine interacts with saline and freshwater. Their studies comprise regional systems of base levels that capture water, which is subject to high evaporation rates and where the density driven brine underlies lower salinity water and displaces saline water flowing tens of kilometres from the source. And although the geologic setting is different, the resulting concentration configurations show a similar pattern.

The results show that the climatic parameters are very important in controlling the hydrogeological configuration. This points to the fact that the system of the freshwater lens is dominated by rainfall and evapotranspiration events and is therefore sensitive to changes in either of these parameters. It is therefore also very sensitive to increased extraction rates.

The future scenarios of climate change indicate that hydraulic heads will increase due to sea level rise and decrease due to longer periods of drought. The thickness (in concentration) of the freshwater lens is highly responsive to both events, generating a deeper lens (+2 m) with sea level rise and a thinner lens (–3 m) due to lower precipitation and higher evapotranspiration rates.

The horizontal extent of the model was perhaps too ambitious considering that extensive field data is only available for the sand bar section where the freshwater lens develops, but it is necessary and essential to have proper boundary conditions in the area of interest e.g. the freshwater lens. Therefore the reliability of this model is questionable due to several assumptions that were considered. Nevertheless, in reality it is difficult to account for such spatially extensive field data and in this light, such a model can be useful to better comprehend the processes that occur in coastal aquifers. However, as a predictive tool, more extensive regional data is needed to calibrate the model in areas where there is little or no knowledge of hydrogeological processes. For predictive purposes, a smaller scale model including only the freshwater lens and immediate boundaries would perhaps have been more suitable. However, this only works when proper boundary conditions are implemented; if there is uncertainty as to these boundaries, then a larger model is conceptually better.

During the model runs, the freshwater lens grew and contracted slightly. However, in the field the freshwater lens varies abruptly between seasons. This is difficult to model with seasonal stress periods of several months and realistic values of recharge and evapotranspiration. In order to develop a precise model of the area of the sand bar, a smaller scale model, encompassing only the sand bar and immediate boundaries would better suit this purpose.

The dilution of salinity observed in the salinity profiles in this work is not implemented in the model scenarios. In the model, the brine concentration displaces the initial salt domain and remains brine for the duration of the simulation. This, however, is not what appears to happen in the field. In the field there is some seasonal dilution of salinity, which could be caused by several factors including: freshwater pockets between loam and clay intervals and regional groundwater flow from the mountains. In either case, it remains an uncertainty in the model that can only be answered with more detailed research of the area.

The 2D approach of this study has limitations on the top boundaries of the model, particularly in the lagoon boundary, since here it is assumed that the lagoon and wetland system is one single continuous strip in the top layer, which leads to likely overestimations in brine inflow. A 3D case could have perhaps simulated this more realistically, by including patches of land where precipitation and evapotranspiration can take place, thus reducing the volume of brine that flows into the system.

The resulting concentration configurations in scenarios 1, 2 and 3 are a result of water that is directly added and removed from the water table and although this may not be an unrealistic assumption considering that the aquifer is phreatic with shallow water levels, in reality there will be infiltration and percolation and evapotranspiration through plant roots, yielding a more dynamic freshwater lens which varies in concentration and head at every moment in time. Additionally, in the field data, the fresh-saline-brine interface is very thin, in particular closer to the lagoon boundary.

Another effect that is difficult to simulate is the highly dynamic mixing zone that underlies the freshwater lens, where brine concentrations seasonally underlie less salty water in a varying interval of 2-20 meters.

In this work, the size and shape of the freshwater lens is mainly dependent on recharge and evapotranspiration volumes. Nevertheless, other factors may also play a significant role, such as the presence of low permeability layers and higher sea levels (Post & Simmons, 2010; Oude Essink et al, 2010 in Mollema & Antonellini, 2013). Additionally, Post & Simmons (2010) indicate that salinization can also occur due to convective bottom-up processes in low permeability strata. These convective upward flows can be observed during the dry season in all modelled scenarios of this study.

In groundwater modelling, when two adjacent zones with relatively large differences in concentration are modelled, e.g. contact between freshwater and seawater or between freshwater and brine, instabilities in the numerical simulation will occur. This is due to the solution of the flow and transport equations at the end of every time step, where new concentrations and densities are determined. Consequently, abrupt changes in density between adjacent cells will lead to unrealistically large velocity vectors at the boundaries. This is a common issue in many density dependent groundwater models.

All these observations point to the complexity of simulating natural processes via numerical computer models. An important observation is that a highly complex model, with many parameters and fluxes does not necessarily represent the real transient dynamic nature of physical processes. It is therefore more important to make a numerical model as simple as possible, taking into account only the most important processes and factors. A complicated model can lead to more confusion and less understanding. However, numerical models can be useful in the sense that they challenge the knowledge of hydrogeologists in understanding the natural system and in the discrimination between the most important parameters that occur within the system.

To resolve the assumptions and uncertainties of this model and to verify some of the field data, further research, including: long duration pumping tests (2 to 4 days) located in the marine, lagoon and central portions of the aquifer to obtain hydraulic parameters for the entire area, piezometric seasonal studies in the lagoon, deeper observation wells in the freshwater lens with continual head and concentration measurements and more accurate local rainfall and evapotranspiration data in the

study area is needed to provide a more accurate water system analysis and stronger data extensive foundation for numerical modelling requirements.
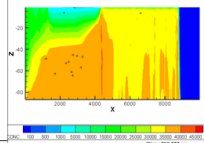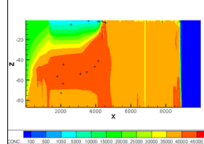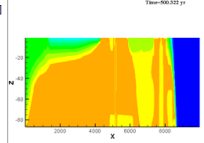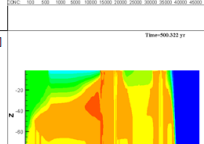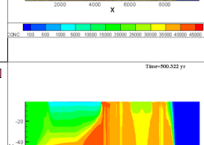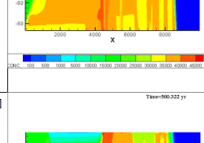
VII. References
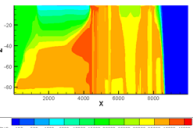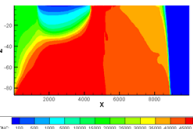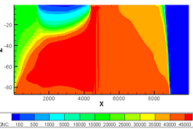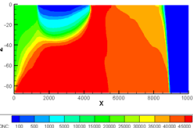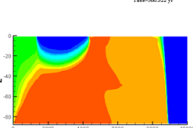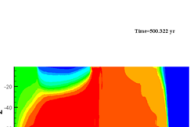
Allaby, M. 2008. Oxford Dictionary of Earth Sciences. 3rd ed. Oxford University Press.

Bear, J. 1972. Dynamics of fluids in porous media, American Elsevier Publishing Company, Inc. New York.

CNA. 2009. Actualización de la disponibilidad media anual de agua subterránea, Acuífero (2512) Laguna Agua Grande, Estado de Sinaloa. Subdirección General Técnica. Gerencia de Aguas Subterráneas. (in Spanish). Mexico.

COPEI *Ingeniería*. 2011. *Estudios hidrogeológicos para complementar los requerimientos de la norma aplicable (NOM-014-CONAGUA-2007) y anteproyecto de sistema de recarga (SRA) para el centro integralmente planeado Costa Pacífico, en el Estado de Sinaloa. Informe Final. Dirección Adjunta de Desarrollo, Subdirección de Promoción de Desarrollo, Gerencia de Infraestructura.* FONATUR, Mexico.

Custodio E. & Llamas, M.R. 1976. Hidrología subterránea. (in Spanish) Ed. Omega. Barcelona. Spain.

Custodio, E. & Bruggeman, G.A. 1987. Groundwater problems in coastal areas. UNESCO. Belgium.

de Louw, P.G.B., Eeman, S., Siemon, B., Voortman, B.R., Gunnink, J., van Baaren, E.S., Oude Essink, G.H.P. 2011. Shallow rainwater lenses in deltaic areas with saline seepage. Hydrology and Earth System Sciences, 15, 3659-3678.

Harbaugh, A.W. & McDonald, M.G. 1996. User's documentation for the U.S. Geological Survey modular finite-difference ground-water flow model. U.S.G.S. Open-File Report 96-485, 56 pp.

Hem, J.D. 1985. Study and Interpretation of the Chemical Characteristics of Natural Water. 3rd ed. USGS Water Supply Paper 2254.

Hiscock, K.M. 2005. Hydrogeology: principles and practice. Blackwell Publishing. UK.

IPCC, 2011. Contribution of Working Group I to the Fourth Assessment Report of the Intergovernmental Panel on Climate Change. Solomon, S., D. Qin, M. Manning, Z. Chen, M. Marquis, K.B. Averyt, M. Tignor and H.L. Miller (eds.). Cambridge University Press, Cambridge, United Kingdom and New York, NY, USA.

IPCC. 2013. Climate Change 2013: The Physical Science Basis. Contribution of Working Group I to the Fifth Assessment Report of the Intergovernmental Panel on Climate Change [Stocker, T.F., D. Qin, G.-K. Plattner, M. Tignor, S.K. Allen, J. Boschung, A. Nauels, Y. Xia, V. Bex and P.M. Midgley (eds.)]. Cambridge University Press, Cambridge, United Kingdom and New York, NY, USA, 1535 pp.

Kafri, U., Shalev, E., Lyakhovsky, V., Wollman, S., Yechieli, Y. 2013. Numerical modelling of seawater intrusion into endorheic hydrological systems. Hydrogeology Journal. doi:10.1007/978-3-642-13944-4.

Karmalkar, A.V., Bradley, R.S., Diaz, H.F. 2011. Climate change in Central America and Mexico: regional climate model validation and climate change projections. Climate Dynamics. Vol. 37. Issue 3-4. pp. 605-629. doi: 10.1007/s00382-011-1099-9.

Konikow, L.F., Goode, D.J. & Hornberger, G.Z. 1996. A three-dimensional method-of-characteristics solute-transport model (MOC3D). U.S.G.S. Water-Resources Investigations Report 96-4267, 87 pp.
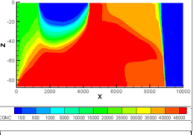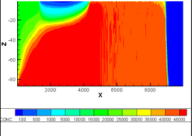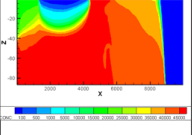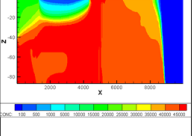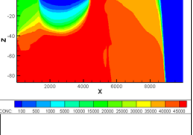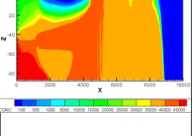
McDonald, M.G. & Harbaugh, A.W. 1988. A Modular Three-Dimensional Finite-Difference Groundwater Flow Model. Techniques of Water-Resources Investigations of the U.S.G.S. Chapter A1. pp. 83-875.

Mollema, P.N. & Antonellini, M. 2013. Seasonal variation in natural recharge of coastal aquifers. Hydrogeology Journal 21:787-797.

Oberdorfer, J.A. 2003. Hydrogeologic modeling of submarine groundwater discharge: comparison to other quantitative methods. Biogeochemistry 66: 159-169.

Oude Essink, G.H.P. 2000. Groundwater Modelling. Lecture Notes, Utrecht University. The Netherlands.

Oude Essink, G.H.P. 2001. Density Dependent Groundwater Flow: Saltwater Intrusion and Heat Transport. Lecture Notes, Utrecht University. The Netherlands.

Oude Essink, G.H.P. 1998. MOC3D adapted to simulate 3D density-dependent groundwater flow, In: Proc. of the MODFLOW'98 Conf. Golden, Colorado, USA, 291-303.

Oude Essink, G.H.P. 1999. Simulating density dependent groundwater flow: the adapted MOC3D, In: Proc. of the 15th Salt Water Intrusion Meeting, Ghent, Belgium, May 1998, 69-79.

Oude Essink, G.H.P., van Baaren, E.S., de Louw, P.G.B. 2010. Effects of climate change on coastal groundwater systems: A modelling study in the Netherlands. Water Resources Research, Vol. 46, W00F04.

Post, V., Kooi, H., Simmons, C. 2007. Using hydraulic head measurements in variable-density groundwater flow analyses. Groundwater. Vol. 45. No. 6. pp. 664-671.

Post, V.E.A. & Simmons, C.T. 2010. Free convective controls on sequestration of salts into low-permeability strata: insights from sand tank laboratory experiments and numerical modelling. Hydrogeology Journal 18: 39-54.

Rosado de Palacio, C. 2012. Hydrogeological characterization of the Laguna Grande Coastal Aquifer in Sinaloa, Mexico. BSc thesis. UNAM. Mexico.

Sanford, W.E. & Pope, J.P. 2010. Current challenges using models to forecast seawater intrusion: lessons from the Eastern Shore of Virginia, USA. Hydrogeology Journal 18: 73-93.

SEMARNAT, 2010. *CIP Costa Pacifico. Manifestación de Impacto Ambiental Regional*. Mexico.

Thiery, D. 2004. Saltwater intrusion modelling with an efficient multiphase approach: theory and several field applications. 18th Salt Water Intrusion Meeting (SWIM). Cartagena, Spain.

Visser, M. 2012. Aquifer Storage and Recovery in a Fossil Creek Bed: Managing Droughts in a Brackish Environment. Master of Science Thesis. Utrecht University. The Netherlands.

Werner, A.D., Bakker, M., Post, V.E.A., Vandenbohede, A., Lu, C., Ataie-Ashtiani, B., Simmons, C., Barry, D.A. 2013. Seawater intrusion processes, investigation and management: Recent advances and future challenges. Advances in Water Resources 51: 3-26.

Zimmermann, S., Bauer, P., Held, R., Kinzelbach, W., Walther, J.H. 2006. Salt transport on islands in the Okavango Delta: Numerical investigations. Advances in Water Resources 29: 11-29.

Annexes

Annex 1. Different model parameters and values and resulting scenarios.

Properties/Input files	Tot mod time [yr]	bas	i (row)	j (col)	k (lay)	Head on the boundary (m)	Conductance	Concentration (mgCl⁻/L)	bcf	wel	mocmain	densin	Tecplot result (last Sp)	Notes
Model version														
car014c_seasons	500	FREE format Nsp: 1001 Time step: 100 Wet season: 121,75 [d] Dry season: 243,5 [d]				Wet season:			Kh [m/d]: 45 till -20 [m] 25 till -50 [m] 10 till -88 [m] Kv= 0,1*Kh neff: 0,3 till -18 [m] 0,2 till -60 [m] 0,1 till -75 [m] 0,2 till -88 [m] Steady state	No, of wells: 398 nx: 2-399 Wet: 0,018 [m3/d] Dry: -0,012 [m3/d] Conc rch: 25 [kg/m3 = mgCl-/L]	CELDIS: 4 αL= 0,2 αTV= 0,02 αTH= 0,02	19000 [mgCl⁻/L]		
			1	1	1 -- 53	0,025	100	19000						
			1	1	173 -- 360	1	100	30000						
			2 -- 22	1	1	Increasing fw φ	100	19000						
			23 -- 44	1	1	Increasing fw φ	100	30000						
						Dry season:								
			1	1	173 -- 360	0,025	100	50000						
car015_seasons	500	FREE format Nsp: 1001 Time step: 100 Wet season: 121,75 [d] Dry season: 243,5 [d]				Wet season:			Kh [m/d]: 45 till -20 [m] 25 till -50 [m] 10 till -88 [m] Kv= 0,1*Kh neff: 0,3 till -18 [m] 0,2 till -60 [m] 0,1 till -75 [m] 0,2 till -88 [m] Steady state	No, of wells: 119 nx: 54-172 Wet: 0,018 [m3/d] Dry: -0,012 [m3/d] Conc rch: 25 [kg/m3 = mgCl-/L]	CELDIS: 4 αL= 0,2 αTV= 0,02 αTH= 0,02	19000 [mgCl⁻/L]		
			1	1	1 -- 53	0,025	100	19000						
			1	1	173 -- 360	1	100	30000						
			2 -- 22	1	1	Increasing fw φ	100	19000						
			23 -- 44	1	1	Increasing fw φ	100	30000						
						Dry season:								
			1	1	173 -- 360	0,025	100	50000						
car016_seasons	500	FREE format Nsp: 1001 Time step: 100 Wet season: 121,75 [d] Dry season: 243,5 [d]				Wet season:			Kh [m/d]: 30 till -20 [m] 20 till -50 [m] 10 till -88 [m] Kv≈ 0,1*Kh In lagoon (i:173-360): Kh: 1, Kv: 0,1 till -4 [m] neff: 0,2 everywhere Steady state	NEW wel package (makewel_Gu) No, of wells: 119 nx: 54-172 Wet-dry period 1961-2008 Wet: + [m3/d] Dry: - [m3/d] Conc rch: 25 [kg/m3 = mgCl-/L]	CELDIS: 4 αL= 0,2 αTV= 0,02 αTH= 0,02	19000 [mgCl⁻/L]		Low k interval in first two layers (-4 m) in lagoon boundary, reproducing fine sediments.
			1	1	1 -- 53	0,025	100	19000						
			1	1	173 -- 360	1	100	30000						
			2 -- 22	1	1	Increasing fw φ	100	19000						
			23 -- 44	1	1	Increasing fw φ	100	30000						
						Dry season:								
			1	1	173 -- 360	0,025	100	50000						
car016b_seasons	500	FREE format Nsp: 1001 Time step: 100 Wet season: 121,75 [d] Dry season: 243,5 [d]				Wet season:			Kh [m/d]: 30 till -20 [m] 20 till -50 [m] 10 till -88 [m] Kv≈ 0,1*Kh In lagoon (i:173-360): Kh: 1, Kv: 0,1 till -4 [m] neff: 0,2 everywhere Steady state	NEW wel package (makewel_Gu) No, of wells: 119 nx: 54-172 Wet-dry period 1961-2008 Wet: + [m3/d] Dry: - [m3/d] Conc rch: 25 [kg/m3 = mgCl-/L]	CELDIS: 4 αL= 0,2 αTV= 0,02 αTH= 0,02	19000 [mgCl⁻/L]		Changing the freshwater head in the laggon from 1 m to 0,51 m, which is an average of wet and dry heads: (1+0,025)/2 = 0,51.
			1	1	1 -- 53	0,025	100	19000						
			1	1	173 -- 360	0,51	100	30000						
			2 -- 22	1	1	Increasing fw φ	100	19000						
			23 -- 44	1	1	Increasing fw φ	100	30000						
						Dry season:								
			1	1	173 -- 360	0,025	100	50000						
car017_seasons	500	FREE format Nsp: 1001 Time step: 100 Wet season: 121,75 [d] Dry season: 243,5 [d]				Wet season:			Kh [m/d]: 30 till -20 [m] 20 till -50 [m] 10 till -88 [m] Kv≈ 0,1*Kh In lagoon (i:173-360): Kh: 1, Kv: 0,1 till -4 [m] neff: 0,2 everywhere Steady state	No, of wells: 119 nx: 54-172 Wet: 0,02 [m3/d] Dry: -0,01 [m3/d] Conc rch: 25 [kg/m3 = mgCl-/L]	CELDIS: 4 αL= 0,2 αTV= 0,02 αTH= 0,02	19000 [mgCl⁻/L]		
			1	1	1 -- 53	0,025	100	19000						
			1	1	173 -- 360	0,51	100	30000						
			2 -- 22	1	1	Increasing fw φ	100	19000						
			23 -- 44	1	1	Increasing fw φ	100	30000						
						Dry season:								
			1	1	173 -- 360	0,025	100	50000						
car017b_seasons	500	FREE format Nsp: 1001 Time step: 100 Wet season: 121,75 [d] Dry season: 243,5 [d]				Wet season:			Kh [m/d]: 30 till -20 [m] 20 till -50 [m] 10 till -88 [m] Kv≈ 0,1*Kh In lagoon (i:173-360): Kh: 1, Kv: 0,1 till -4 [m] neff: 0,2 everywhere Steady state	No, of wells: 119 nx: 54-172 Wet: 0,022 [m3/d] Dry: -0,015 [m3/d] Conc rch: 25 [kg/m3 = mgCl-/L]	CELDIS: 4 αL= 0,2 αTV= 0,02 αTH= 0,02	19000 [mgCl⁻/L]		Adding irrigation return of 50% of pumping rate to the (+) value in the wel file
			1	1	1 -- 53	0,025	100	19000						
			1	1	173 -- 360	0,51	100	30000						
			2 -- 22	1	1	Increasing fw φ	100	19000						
			23 -- 44	1	1	Increasing fw φ	100	30000						
						Dry season:								
			1	1	173 -- 360	0,025	100	50000						

Properties/Input files	Tot mod time [yr]	bas	ghb i (row)	j (col)	k (lay)	Head on the boundary (m)	Conductance	Concentration (mgCl⁻/L)	bcf	wel	mocmain	densin	Tecplot result (last Sp)	Notes
Model version													Last Sp	
car018_seasons	500	FREE format Nsp: 1001 Time step: 100 Wet season: 121,75 [d] Dry season: 243,5 [d]				Wet season:			Kh [m/d]: 30 till -20 [m] 20 till -50 [m] 10 till -88 [m] Kv≈0,1*Kh In lagoon (i:173-360): Kh: 1, Kv: 0,1 till -4 [m] neff: 0,2 everywhere	No, of wells: 119 nx: 54-172 Wet: 0,067 [m3/d] Dry: -0,077 [m3/d] Conc rch: 25 [kg/m3 = mgCl-/L]	CELDIS: 4 αL= 0,2 αTV= 0,02 αTH= 0,02	19000 [mgCl⁻/L]		Used the sum of the rain and ET values for 4 and 8 months respectively. Instead of using average values.
			1	1	1 -- 53	0,025	100	19000						
			1	1	173 -- 360	0,51	100	30000						
			2 -- 22	1	1	Increasing fw φ	100	19000						
			23 -- 44	1	1	Increasing fw φ	100	30000						
						Dry season:								
			1	1	173 -- 360	0,025	100	50000						
car018b_seasons	500	FREE format Nsp: 1001 Time step: 100 Wet season: 121,75 [d] Dry season: 243,5 [d]				Wet season:			Kh [m/d]: 30 till -20 [m] 20 till -50 [m] 10 till -88 [m] Kv≈0,1*Kh In lagoon (i:173-360): Kh: 1, Kv: 0,1 till -4 [m] neff: 0,12	No, of wells: 119 nx: 54-172 Wet: 0,022 [m3/d] Dry: -0,026 [m3/d] Conc rch: 25 [kg/m3 = mgCl-/L]	CELDIS: 4 αL= 0,2 αTV= 0,02 αTH= 0,02	19000 [mgCl⁻/L]		Used the sum of the rain and ET values for 4 and 8 months respectively. Instead of using average values. Values are 1/3 of car018_seasons
			1	1	1 -- 53	0,025	100	19000						
			1	1	173 -- 360	0,51	100	30000						
			2 -- 22	1	1	Increasing fw φ	100	19000						
			23 -- 44	1	1	Increasing fw φ	100	30000						
						Dry season:								
			1	1	173 -- 360	0,025	100	50000						
car018c_seasons	500	FREE format Nsp: 1001 Time step: 100 Wet season: 121,75 [d] Dry season: 243,5 [d]				Wet season:			Kh [m/d]: 30 till -20 [m] 20 till -50 [m] 10 till -88 [m] Kv≈0,1*Kh In lagoon (i:173-360): Kh: 1, Kv: 0,1 till -4 [m] neff: 0,12	No, of wells: 119 nx: 54-172 Wet: 0,018 [m3/d] Dry: -0,022 [m3/d] Conc rch: 25 [kg/m3 = mgCl-/L]	CELDIS: 4 αL= 0,2 αTV= 0,02 αTH= 0,02	19000 [mgCl⁻/L]		
			1	1	1 -- 53	0,025	100	19000						
			1	1	173 -- 360	0,51	100	30000						
			2 -- 22	1	1	Increasing fw φ	100	19000						
			23 -- 44	1	1	Increasing fw φ	100	30000						
						Dry season:								
			1	1	173 -- 360	0,025	100	50000						
Scenario_1	500	FREE format Nsp: 1001 Time step: 100 Wet season: 121,75 [d] Dry season: 243,5 [d]				Wet season:			Kh [m/d]: 30 till -20 [m] 20 till -50 [m] 10 till -88 [m] Kv≈0,1*Kh In lagoon (i:173-360): Kh: 1, Kv: 0,1 till -4 [m] neff: 0,12 everywhere Steady state	No, of wells: 119 nx: 54-172 Wet: 0,027 [m3/d] Dry: -0,027 [m3/d] Conc rch: 25 [kg/m3 = mgCl-/L]	CELDIS: 4 αL= 0,2 αTV= 0,02 αTH= 0,02	19000 [mgCl⁻/L]		Data comes from car018c_seasons
			1	1	1 -- 53	0,025	100	19000						
			1	1	173 -- 360	0,51	100	30000						
			2 -- 22	1	1	Increasing fw φ	100	19000						
			23 -- 44	1	1	Increasing fw φ	100	30000						
						Dry season:								
			1	1	173 -- 360	0,025	100	50000						
Scenario_2	500	FREE format Nsp: 1001 Time step: 100 Wet season: 121,75 [d] Dry season: 243,5 [d]				Wet season:			Kh [m/d]: 30 till -20 [m] 20 till -50 [m] 10 till -88 [m] Kv≈0,1*Kh In lagoon (i:173-360): Kh: 1, Kv: 0,1 till -4 [m] neff: 0,12 everywhere Steady state	No, of wells: 119 nx: 54-172 Wet: 0,02 [m3/d] Dry: -0,01 [m3/d] Conc rch: 25 [kg/m3 = mgCl-/L]	CELDIS: 4 αL= 0,2 αTV= 0,02 αTH= 0,02	19000 [mgCl⁻/L]		Data comes from car018c_seasons
			1	1	1 -- 53	0,025	100	19000						
			1	1	173 -- 360	0,51	100	30000						
			2 -- 22	1	1	Increasing fw φ	100	19000						
			23 -- 44	1	1	Increasing fw φ	100	30000						
						Dry season:								
			1	1	173 -- 360	0,025	100	50000						
Scenario_3	500	FREE format Nsp: 1001 Time step: 100 Wet season: 121,75 [d] Dry season: 243,5 [d]				Wet season:			Kh [m/d]: 60 till -20 [m] 20 till -50 [m] 10 till -88 [m] Kv≈0,1*Kh In lagoon (i:173-360): Kh: 1, Kv: 0,1 till -4 [m] neff: 0,12 everywhere Steady state	No, of wells: 119 nx: 54-172 Wet: 0,027 [m3/d] Dry: -0,027 [m3/d] Conc rch: 25 [kg/m3 = mgCl-/L]	CELDIS: 4 αL= 0,2 αTV= 0,02 αTH= 0,02	19000 [mgCl⁻/L]		Left vertical boundary, from -44 to -88 m.b.s.l, changed from 30 000 to 50 000 mgCl/L. All scenarios that follow incorporate this change.
			1	1	1 -- 53	0,025	100	19000						
			1	1	173 -- 360	0,51	100	30000						
			2 -- 22	1	1	Increasing fw φ	100	19000						
			23 -- 44	1	1	Increasing fw φ	100	50000						
						Dry season:								
			1	1	173 -- 360	0,025	100	50000						

Properties/Input files	Tot mod time [yr]	bas	ghb						bcf	wel	mocmain	densin	Tecplot result (last Sp)	Notes
Model version			i (row)	j (col)	k (lay)	Head on the boundary (m)	Conductance	Concentration (mgCl⁻/L)					Last Sp	
Scenario_4	500	FREE format Nsp: 1001 Time step: 100 Wet season: 121,75 [d] Dry season: 243,5 [d]	Wet season: 1 / 1 / 2 -- 22 / 23 -- 44 ; Dry season: 1	1 / 1 / 1 / 1 ; 1	1 -- 53 / 173 -- 360 / 1 / 1 ; 173 -- 360	0,025 / 0,51 / Increasing fw φ / Increasing fw φ ; 0,025	100 / 100 / 100 / 100 ; 100	19000 / 30000 / 19000 / 50000 ; 50000	Kh [m/d]: 10 till -20 [m] 20 till -50 [m] 10 till - 88 [m] Kv= 0,1*Kh In lagoon (i:173-360): Kh: 1, Kv: 0,1 till -4 [m] neff: 0,12 everywhere Steady state	No, of wells: 119 nx: 54-172 Wet: 0,027 [m3/d] Dry: -0,027 [m3/d] Conc rch: 25 [kg/m3 = mgCl-/L]	CELDIS: 4 αL= 0,2 αTV= 0,02 αTH= 0,02	19000 [mgCl⁻/L]		Kh from 60 m/d to 10 m/d in the first -20m. The thickness of the freshwater lens increases considerably.
Scenario_5	500	FREE format Nsp: 1001 Time step: 100 Wet season: 121,75 [d] Dry season: 243,5 [d]	Wet season: 1 / 1 / 2 -- 22 / 23 -- 44 ; Dry season: 1	1 / 1 / 1 / 1 ; 1	1 -- 53 / 173 -- 360 / 1 / 1 ; 173 -- 360	0,025 / 0,51 / Increasing fw φ / Increasing fw φ ; 0,025	100 / 100 / 100 / 100 ; 100	19000 / 30000 / 19000 / 50000 ; 50000	Kh [m/d]: 60 till -20 [m] 20 till -50 [m] 10 till - 88 [m] Kv= 0,1*Kh neff: 0,12 everywhere Steady state	No, of wells: 119 nx: 54-172 Wet: 0,027 [m3/d] Dry: -0,027 [m3/d] Conc rch: 25 [kg/m3 = mgCl-/L]	CELDIS: 4 αL= 0,2 αTV= 0,02 αTH= 0,02	19000 [mgCl⁻/L]		This scenario shows the effect of removing the low k interval in the lagoon.
Scenario_6	500	FREE format Nsp: 1001 Time step: 100 Wet season: 121,75 [d] Dry season: 243,5 [d]	Wet season: 1 / 1 / 2 -- 22 / 23 -- 44 ; Dry season: 1	1 / 1 / 1 / 1 ; 1	1 -- 53 / 173 -- 360 / 1 / 1 ; 173 -- 360	0,025 / 0,51 / Increasing fw φ / Increasing fw φ ; 0,025	100 / 100 / 100 / 100 ; 100	19000 / 30000 / 19000 / 50000 ; 50000	Kh [m/d]: 30 till -20 [m] 20 till -50 [m] 10 till - 88 [m] Kv= 0,1*Kh In lagoon (i:173-360): Kh: 1, Kv: 0,1 till -4 [m] neff: 0,12 everywhere Steady state	No, of wells: 119 nx: 54-172 Wet: 0,027 [m3/d] Dry: -0,027 [m3/d] Conc rch: 25 [kg/m3 = mgCl-/L]	CELDIS: 4 αL= 0,2 αTV= 0,02 αTH= 0,02	19000 [mgCl⁻/L]		Correction of the freshwater head calculation on the GHB package in the left vertical sea boundary. All scenarios that follow incorporate this change.
Scenario_7 (Reference case)	500	FREE format Nsp: 1001 Time step: 100 Wet season: 121,75 [d] Dry season: 243,5 [d]	Wet season: 1 / 1 / 2 -- 22 / 23 -- 44 ; Dry season: 1	1 / 1 / 1 / 1 ; 1	1 -- 53 / 173 -- 360 / 1 / 1 ; 173 -- 360	0,025 / 0,51 / Increasing fw φ / Increasing fw φ ; 0,025	100 / 100 / 100 / 100 ; 100	19000 / 30000 / 19000 / 50000 ; 50000	Kh [m/d]: 60 till -20 [m] 20 till -50 [m] 10 till - 88 [m] Kv= 0,1*Kh In lagoon (i:173-360): Kh: 1, Kv: 0,1 till -4 [m] neff: 0,12 everywhere Steady state	No, of wells: 119 nx: 54-172 Wet: 0,027 [m3/d] Dry: -0,027 [m3/d] Conc rch: 25 [kg/m3 = mgCl-/L]	CELDIS: 4 αL= 0,2 αTV= 0,02 αTH= 0,02	19000 [mgCl⁻/L]		Recharge, ET and pumping rates as reported by CNA (2009).
Scenario_8	500	FREE format Nsp: 1001 Time step: 100 Wet season: 121,75 [d] Dry season: 243,5 [d]	Wet season: 1 / 1 / 2 -- 22 / 23 -- 44 ; Dry season: 1	1 / 1 / 1 / 1 ; 1	1 -- 53 / 173 -- 360 / 1 / 1 ; 173 -- 360	0,025 / 0,51 / Increasing fw φ / Increasing fw φ ; 0,025	100 / 100 / 100 / 100 ; 100	19000 / 30000 / 19000 / 50000 ; 50000	Kh [m/d]: 30 till -20 [m] 20 till -50 [m] 10 till - 88 [m] Kv= 0,1*Kh In lagoon (i:173-360): Kh: 1, Kv: 0,1 till -4 [m] neff: 0,12 everywhere Steady state	No, of wells: 119 nx: 54-172 Wet: 0,030 [m3/d] Dry: -0,027 [m3/d] Conc rch: 25 [kg/m3 = mgCl-/L]	CELDIS: 4 αL= 0,2 αTV= 0,02 αTH= 0,02	19000 [mgCl⁻/L]		
Scenario_9	500	FREE format Nsp: 1001 Time step: 100 Wet season: 121,75 [d] Dry season: 243,5 [d]	Wet season: 1 / 1 / 2 -- 22 / 23 -- 44 ; Dry season: 1	1 / 1 / 1 / 1 ; 1	1 -- 53 / 173 -- 360 / 1 / 1 ; 173 -- 360	0,025 / 0,51 / Increasing fw φ / Increasing fw φ ; 0,025	100 / 100 / 100 / 100 ; 100	19000 / 30000 / 19000 / 50000 ; 50000	Kh [m/d]: 60 till -20 [m] 20 till -50 [m] 10 till - 88 [m] Kv= 0,1*Kh In lagoon (i:173-360): Kh: 1, Kv: 0,1 till -4 [m] neff: 0,12 everywhere Steady state	No, of wells: 119 nx: 54-172 Wet: 0,02 [m3/d] Dry: -0,01 [m3/d] Conc rch: 25 [kg/m3 = mgCl-/L]	CELDIS: 4 αL= 0,2 αTV= 0,02 αTH= 0,02	19000 [mgCl⁻/L]		Using Scenario_7 as reference case and changing the values in the Wel file to the measured rain and ET values of the La Concha weather station in 2004.

Properties/Input files	Tot mod time [yr]	bas	ghb						bcf	wel	mocmain	densin	Tecplot result (last Sp)	Notes
Model version			i (row)	j (col)	k (lay)	Head on the boundary (m)	Conductance	Concentration (mgCl⁻/L)					**Last Sp**	
Scenario_10	500	FREE format Nsp: 1001 Time step: 100 Wet season: 121,75 [d] Dry season: 243,5 [d]	\<Wet season:\> 1; 1; 1 -- 53; 0,025; 100; 19000 | 1; 1; 173 -- 360; 0,51; 100; 30000 | 2 -- 22; 1; 1; Increasing fw φ; 100; 19000 | 23 -- 44; 1; 1; Increasing fw φ; 100; 50000 | \<Dry season:\> 1; 1; 173 -- 360; 0,025; 100; 50000						Kh [m/d]: 60 till -20 [m] 20 till -50 [m] 10 till -88 [m] Kv≈0,1*Kh In lagoon (i:173-360): Kh: 1, Kv: 0,1 till -4 [m] neff: 0,12 everywhere Steady state	NEW wel package (makewel_Gu) No, of wells: 119 nx: 54-172 Wet-dry period 1961-2008 Wet: + [m3/d] Dry: - [m3/d] Conc rch: 25 [kg/m3 = mgCl-/L]	CELDIS: 4 αL= 0,2 αTV= 0,02 αTH= 0,02	19000 [mgCl⁻/L]		Using Scenario_7 as reference case and changing the values in the Wel file to the measured rain and ET values of the La Concha weather station from 1968-2008 as a loop of 38 yrs (there are no measurements for some years) that repeats until 500 yrs.
Reference case + Sea level rise	500	FREE format Nsp: 1001 Time step: 100 Wet season: 121,75 [d] Dry season: 243,5 [d]	\<Wet season:\> 1; 1; 1 -- 53; 0,08; 100; 19000 | 1; 1; 173 -- 360; 0,51; 100; 30000 | 2 -- 22; 1; 1; Increasing fw φ; 100; 19000 | 23 -- 44; 1; 1; Increasing fw φ; 100; 50000 | \<Dry season:\> 1; 1; 173 -- 360; 0,08; 100; 50000						Kh [m/d]: 60 till -20 [m] 20 till -50 [m] 10 till -88 [m] Kv≈0,1*Kh In lagoon (i:173-360): Kh: 1, Kv: 0,1 till -4 [m] neff: 0,12 everywhere Steady state	No, of wells: 119 nx: 54-172 Wet: 0,027 [m3/d] Dry: -0,027 [m3/d] Conc rch: 25 [kg/m3 = mgCl-/L]	CELDIS: 4 αL= 0,2 αTV= 0,02 αTH= 0,02	19000 [mgCl⁻/L]		Future scenario including 0,80 m of sea level rise.
Reference case + drought	500	FREE format Nsp: 1001 Time step: 100 Wet season: 121,75 [d] Dry season: 243,5 [d]	\<Wet season:\> 1; 1; 1 -- 53; 0,025; 100; 19000 | 1; 1; 173 -- 360; 0,51; 100; 30000 | 2 -- 22; 1; 1; Increasing fw φ; 100; 19000 | 23 -- 44; 1; 1; Increasing fw φ; 100; 50000 | \<Dry season:\> 1; 1; 173 -- 360; 0,025; 100; 50000						Kh [m/d]: 60 till -20 [m] 20 till -50 [m] 10 till -88 [m] Kv≈0,1*Kh In lagoon (i:173-360): Kh: 1, Kv: 0,1 till -4 [m] neff: 0,12 everywhere Steady state	No, of wells: 119 nx: 54-172 Wet: 0,027 [m3/d] Dry: -0,027 [m3/d] Conc rch: 25 [kg/m3 = mgCl-/L]	CELDIS: 4 αL= 0,2 αTV= 0,02 αTH= 0,02	19000 [mgCl⁻/L]		Future scenario including an increase of 20% in evapotranspiration.
Reference case + Sea level rise & drought	500	FREE format Nsp: 1001 Time step: 100 Wet season: 121,75 [d] Dry season: 243,5 [d]	\<Wet season:\> 1; 1; 1 -- 53; 0,08; 100; 19000 | 1; 1; 173 -- 360; 0,51; 100; 30000 | 2 -- 22; 1; 1; Increasing fw φ; 100; 19000 | 23 -- 44; 1; 1; Increasing fw φ; 100; 50000 | \<Dry season:\> 1; 1; 173 -- 360; 0,08; 100; 50000						Kh [m/d]: 60 till -20 [m] 20 till -50 [m] 10 till -88 [m] Kv≈0,1*Kh In lagoon (i:173-360): Kh: 1, Kv: 0,1 till -4 [m] neff: 0,12 everywhere Steady state	No, of wells: 119 nx: 54-172 Wet: 0,027 [m3/d] Dry: -0,032 [m3/d] Conc rch: 25 [kg/m3 = mgCl-/L]	CELDIS: 4 αL= 0,2 αTV= 0,02 αTH= 0,02	19000 [mgCl⁻/L]		Future scenario including 0,80 m of sea level rise and an increase of 20% in evapotranspiration.

Annex 2. EC values in salinity profiles in wells B1, B2 and B3 during different measurement periods.

EC range

< 2000	(blue)
2000-10000	(yellow)
10001-54000	(orange)
> 54000	(red)

Well B1, close to coastline

Depth	May-09	Aug-09	Oct-09	Dec-09	Mar-10	Apr-10	Jun-10	Aug-10	Mar-11	Apr-11	Aug-11
	EC	EC	EC	EC	EC	EC	EC	EC	EC	EC	EC
(m)	(µS/cm)	(µS/cm)	(µS/cm)	(µS/cm)	(µS/cm)	(µS/cm)	(µS/cm)	(µS/cm)	(µS/cm)	(µS/cm)	(µS/cm)
wt	1570	778	470	640	671	672	595	467	805	795	707
2,00					675	679	594	474	805	782	819
3,00					680		679	487	808	788	786
4,00			600		680	690	689	494	822	801	799
5,00	1588	742		700	702		788	532	842	804	801
6,00					702	710	1350	664	855	1600	802
7,00		1590	1200	788	1570		4540	1080	1850	3050	942
8,00					4180	4250	9330	2650	4024	5520	1495
9,00					7580		12200	4680	8000	8690	3710
10,00	1855	4730	5370	8200	10490	10600	14440	5330	10370	11300	6730
11,00	2218	8610		10650	13600		16100	6400	12950	13820	9610
12,00	2405	10180		13030	14400	14500	18200	7200	14270	14710	10900
13,00	3578	11800		13120	14590		17700	7470	14370	14980	11130
14,00	4455	12790		13280	14820	14950	17800	7680	14500	14600	11400
15,00	5375	12690		13480	14860		18900	7700	14400	15600	11450
16,00				13370	15100	15300	18200	7700	14520	15300	11540
17,00		16600	10330	13290	14890		18700		14520	14500	11290
18,00		22300		13000	14670	15500	17500		14670	15600	15900
19,00		23400		13250	14780		17900		14520	15800	16600
20,00	6955	25300	10400	13440	14980	15700	18200		14460	15200	17800
SL	1,55	1,33	0,68	1,13	1,15	1,14	1,52	0,95	1,06	1,19	0,86
FWL	6,45	5,67	7,32	6,87	6,85	5,86	5,48	7,05	6,94	6,81	7,14

wt	Water table depth	Dry season	March-June
SL	Static level (water table depth)	Wet season	July-August
FWL	Fresh water lens thickness		

EC range

< 2000	(blue)
2000-10000	(yellow)
10001-54000	(orange)
> 54000	(red)

Well B3, close to lagoon

Depth	May-09	Aug-09	Oct-09	Dec-09	Mar-10	Apr-10	Jun-10	Aug-10	Mar-11	Apr-11	Aug-11
	EC	EC	EC	EC	EC	EC	EC	EC	EC	EC	EC
(m)	(µS/cm)	(µS/cm)	(µS/cm)	(µS/cm)	(µS/cm)	(µS/cm)	(µS/cm)	(µS/cm)	(µS/cm)	(µS/cm)	(µS/cm)
wt	800	566	210	294	340		307	179	360	403	742
3,00					428			184	383	410	735
4,00					431	501	466	265	391	415	801
5,00	1325	786	510	448	429		472	342	394	2910	1231
6,00	2650	3730		7988	2870	2920	2500	1690	326	15700	3040
7,00	10350	16700		11600	16100		14900	7650	13500	26200	13870
8,00	10550			30660	27800	28400	27200	12480	25800	35400	22900
9,00	11000	37900	35217	46760	35900		34400	15570	33200	82500	33100
10,00	42500	>100000	80160	72000	78300	79200	77800	> 20000	75900	100000	69900
11,00		>100000			92100		>100000	> 20000	91700	>100000	100000
12,00		>100000		89160	93000	93400	>100000	>100000	96900	>100000	>100000
13,00		>100000			94400		>100000	>100000	98300	>100000	>100000
14,00		>100000			95500	94500	>100000	>100000	99700	>100000	>100000
15,00	47750	>100000	101960	>100000	96400		>100000	>100000	100000	>100000	>100000
16,00		>100000		>100000	96400	95800	>100000	>100000	>100000	>100000	>100000
17,00		>100000		>100000	96900		>100000	>100000	>100000	>100000	>100000
18,00		>100000		>100000	99000	98200	>100000	>100000	>100000	>100000	>100000
19,00		>100000		>100000	>100000		>100000	>100000	>100000	>100000	>100000
20,00	51500	>100000	110850	>100000	>100000	99000	>100000	>100000	>100000	>100000	>100000
SL	2,61	2,37	1,65	2,1	2,06	2,09	2,53	2,04	2,32	2,46	2,09
FWL	2,39	2,63	3,35	2,9	2,94	2,91	2,47	3,96	3,68	3,54	3,91

wt	Water table depth	Dry season	March-June
SL	Static level (water table depth)	Wet season	July-August
FWL	Fresh water lens thickness		

EC range

(blue)	< 2000
(yellow)	2000-10000
(orange)	10001-54000
(red)	> 54000

Well B2, Centre of the sand bar

Depth (m)	May-09 EC (µS/cm)	Aug-09 EC (µS/cm)	Oct-09 EC (µS/cm)	Dec-09 EC (µS/cm)	Mar-10 EC (µS/cm)	Apr-10 EC (µS/cm)	Jun-10 EC (µS/cm)	Aug-10 EC (µS/cm)	Mar-11 EC (µS/cm)	Apr-11 EC (µS/cm)	Aug-11 EC (µS/cm)
wt	27500	2340	2500	1200	1600	1610	1421	767	1860	1910	1420
2,00		2378	2600	1170	1600		1449	1010	1870	1930	2080
3,00		8730		1200	1610		1497	1067	1890	1920	2120
4,00		58500		1150	1650	1609	1570	1064	1920	1920	2150
5,00	28750	61000	7920	1150	1650		1610	1078	1840	1970	2310
6,00					1780	1774	1630	1331	1960	6310	2420
7,00					5570		4840	2360	5320	11440	2930
8,00					9700	9800	12070	3490	9820	13900	3330
9,00					11200		69900	6000	13090	22000	8860
10,00	29400	61600		42700	22800	23100	70300	10670	17900	45900	13580
11,00					58300		70200	> 20000	46100	46900	16400
12,00					58900	58900	70600	> 20000	48900	47800	17700
13,00					59100		69900	> 20000	48900	47900	20000
14,00					59900	59000	69000	> 20000	49700	48100	23300
15,00	29700	61500		59200	59700		69700	> 20000	49100	47900	29700
16,00					61000	59500	69700		48100	48700	36700
17,00					59600		70100		49700	48900	58600
18,00					59700	59800	70600		49600	51200	59900
19,00					59300		70900		50200	59500	62000
20,00	29900	61500		76400	60000	60100	71100		52000	82200	66800
21,00					78200		70000		82300	83500	68600
22,00					79000	78800	70300		82400	84200	69000
23,00					80000		71000		83000	85300	68900
24,00					81000	81500	71500		84500	88000	68700
25,00	30150	61400		96900	82000		70000		83900	91500	69500
26,00					83000	82200	70500		86900	97300	69900
27,00					84600		69600		93000	98500	70600
28,00					92200	89800	70100		98600	99000	70900
29,00					98000		69900		98200	99300	72400
30,00	30350	61400	125640		98500	92500	70400		99100	100000	71500
31,00					99000		70700		100000	>100000	72100
32,00					99700	94400	70600		99800	>100000	73200
33,00					99100		69800		98400	>100000	71700
34,00					99800	95900	69000		99000	>100000	69900
35,00		54400		>100000	99800		69400		99600	>100000	71500
36,00					99800	97000	64100		99300	>100000	66600
37,00					99800		61500		99400	>100000	60800
38,00					99200	98500	58400		98300	>100000	57900
39,00					99500		56400		98500	>100000	56600
40,00		51200	120435	>100000	99800	98700	54600		99100	>100000	53700
41,00					98100		53000		99000	>100000	55100
42,00					96400	98800	53800		99000	>100000	55400
43,00					89000		54300		97700	>100000	53700
44,00					84100	87100	54000		98000	>100000	53800
45,00		50400		>100000	77000		53100		97100	>100000	52200
46,00					67000	79000	53300		96100	>100000	54100
47,00					60700		50700		94100	>100000	52300
48,00					52900	65500	49600		93700	>100000	53400
49,00					49000		47000		92200	>100000	52900
50,00		44900	122062	>100000	47900	53200	48100		91300	>100000	53000
51,00					47100		47200		91500	>100000	50900
52,00					47000	50000	47500		90400	>100000	51300
53,00					45800		46400		92100	>100000	53400
54,00					46500	48300	46500		91700	>100000	50900
55,00		44600		>100000	46000		47400		93100	>100000	51300
56,00					47110		48100		95400	>100000	56100
57,00					64900		53900		95400	>100000	69000
58,00					69800		55300		94600	>100000	79400
59,00					70000		52700		97300	>100000	79900
60,00		44000	101165	>100000	42700				93200	>100000	80500
SL	1,45	1,55	0,8	1,13	1,2	1,22	1,56	0,99	1,2	1,35	1,1
FWL	0,00	0,00	0,00	3,87	3,80	3,78	4,44	5,01	4,80	4,65	0,00

wt — Water table depth
SL — Static level (water table depth)
FWL — Fresh water lens thickness

Dry season — March-June
Wet season — July-August